AIMS Environmental Science

AIMS Environmental Science, 13(5): 828–864.
DOI: 10.3934/environsci.2026033
Received: 22 July 2026
Revised: 11 September 2026
Accepted: 16 September 2026
Published: 21 September 2026

https://www.aimspress.com/journal/environmental

Research article

Direct Blue 71 removal by tamarind shell-supported *Phanerochaete chrysosporium*: synergistic biosorption and biodegradation in batch and fixed-bed systems

Ana Dilia Mota-Gutiérrez[1], Raúl Cortés-Martínez[2,*], Ruth Alfaro-Cuevas-Villanueva[2], Orlando Hernández-Cristóbal[3] and Karla Gabriela Domínguez-González[2]

[1] Student of the Master's Program in Biological Sciences, Facultad de Biología, Universidad Michoacana de San Nicolás de Hidalgo, C.U., CP 58030, Morelia, Michoacán, México.
[2] Instituto de Investigaciones en Ciencias de la Tierra, Universidad Michoacana de San Nicolás de Hidalgo. C.U., CP 58030, Morelia, Michoacán, México
[3] Escuela Nacional de Estudios Superiores (ENES), Unidad Morelia, UNAM. Antigua Carretera a Pátzcuaro 8701, col. Ex Hacienda San José de la Huerta, Morelia 58190, Michoacán, México.

* **Correspondence:** Email: raul.cortes@umich.mx; Tel: +524434096372.

Abstract: The increasing discharge of textile dyes into water bodies poses significant environmental and public health challenges. This study developed and evaluated a synergistic system to remove Direct Blue 71 (DB71), a recalcitrant triazo dye, from aqueous solutions by combining biosorption onto tamarind shell (*Tamarindus indica*, TS) with biodegradation by *Phanerochaete chrysosporium* (Pc) immobilized on TS. Both individual and combined systems (TS+Pc) were assessed in batch and continuous fixed-bed column configurations. FTIR and SEM-EDS analyses confirmed that TS has a porous, heterogeneous surface rich in hydroxyl, carboxyl, carbonyl, and amino functional groups; post-adsorption detection of sulfur, absent in the untreated material and attributable only to the dye's sulfonate groups, provided direct evidence of DB71 binding. The pseudo-second-order model best described biosorption kinetics. Maximum DB71 removal (69%) was achieved at pH 3 with a biosorbent dose of 20 g/L, with ~54% still removed at near-neutral pH 7, indicating effective operation without strong acidification. The equilibrium data in the concentration range studied were best fitted by the Freundlich model at 25 and 35 °C and by the Langmuir model at 40 °C, in line with adsorption

on an energetically heterogeneous surface. Since no saturation plateau was obtained, the fitted Langmuir Q_o (13.66 mg/g at 25 °C and 15.73 mg/g at 40 °C) represents an operational capacity for this range rather than a monolayer capacity. Thermodynamic analysis indicated a spontaneous process ($\Delta G° = -33.3$ to -35.5 kJ/mol), with uptake increasing with temperature. *P. chrysosporium* successfully colonized TS within 6–7 days and decolorized DB71 on both nutrient-rich and nutrient-free solid media. In batch experiments, the TS+Pc system achieved decolorization efficiencies of 98%, 76%, and 67% at DB71 concentrations of 10, 50, and 100 mg/L, respectively, substantially outperforming the fungus alone (68%, 49%, and 16%). In fixed-bed columns, inoculation of TS with *Pc* extended the breakthrough time from 25 to 82 min and increased the bed capacity at breakthrough from 2.51 to 8.39 µg/g, a 3.3-fold gain, with the Yoon-Nelson model providing an adequate operational description of the column dynamics ($R^2 = 0.9928$). These results demonstrate that tamarind shell functions simultaneously as a primary biosorbent and a nutrient-rich substrate that sustains fungal ligninolytic activity, yielding a synergistic, low-cost, and sustainable approach for treating azo dye–contaminated textile wastewater.

Keywords: Direct Blue 71; tamarind shell; *Phanerochaete chrysosporium*; biosorption; biodegradation; fixed-bed column; azo dye; textile wastewater

1. Introduction

The textile industry is one of the largest consumers of water worldwide and, consequently, a significant source of water pollution. During dyeing, it is estimated that 10%–15% of synthetic dyes fail to fix to fibers and are discharged into effluents, causing severe visual and chemical pollution. Moreover, some dye classes (direct, vat, sulfur, or disperse dyes) typically exhibit intermediate fixation rates (20%–40% loss, depending on the fiber and process) [1,2]. Among these compounds, azo dyes, characterized by one or more azo bonds (−N=N−), are particularly problematic due to their high chemical stability, recalcitrance to degradation, and the carcinogenic and mutagenic potential of the aromatic amines formed upon their decomposition [3]. In particular, Direct Blue 71 (DB71), a triazo dye with the chemical formula $C_{40}H_{23}N_7Na_4O_{13}S_4$, is widely used to dye cellulose fibers such as cotton in denim manufacturing and poses a significant challenge for water treatment systems [4,5].

Conventional physicochemical methods for color removal, such as coagulation-flocculation, activated carbon adsorption, and advanced oxidation, often have significant disadvantages. These methods can be expensive, consume large amounts of energy, and generate toxic byproducts or sludge that require further treatment. Activated carbon adsorption is highly effective, but its high production and regeneration costs limit its large-scale application, driving the search for low-cost alternative adsorbents [6]. In this context, the principles of sustainable chemistry and circular economy promote the valorization of agricultural residues as biosorbents. These materials are abundant, inexpensive, and renewable [7]. Recent work illustrates the range of strategies available within this waste-to-resource framework: carbon derived from rubber fruit shells has been carbonized, magnetite-coated, and silanized to enhance its affinity for synthetic dyes [8], while rice husk char has been used as a support for Mg–Al layered double hydroxide, with the environmental burden of the synthesis quantified by life cycle assessment [9]. In both cases, the residue is subjected to thermal and chemical modification

before use. This work takes a complementary approach by applying the residue without such treatment. Tamarind shells (*Tamarindus indica L.*), a massive byproduct of the food industry, are a lignocellulosic material rich in cellulose, hemicellulose, and lignin [10] and possess functional groups such as hydroxyls, carboxyls, and esters [11], making them ideal for the adsorption of polar contaminants, such as anionic dyes.

In parallel, bioremediation using microorganisms offers an environmentally friendly alternative for the complete mineralization of organic contaminants. White-rot fungi, such as *Phanerochaete chrysosporium*, are particularly effective due to their nonspecific extracellular enzyme system, composed primarily of lignin peroxidase (LiP), manganese peroxidase (MnP), and laccases [12]. These enzymes generate highly reactive free radicals that can attack and degrade complex, recalcitrant molecular structures, such as those of azo dyes [13]. However, using free-flowing fungal biomass in large-scale reactors presents challenges, including separating biomass from the treated effluent and potential inhibition of fungal growth by high contaminant concentrations [14]. Thus, immobilizing fungal biomass on solid supports can overcome these limitations, improving biocatalyst stability and enabling use in continuous-flow reactor systems [15]. While various support materials have been explored, most are inert. The research gap and the novelty of this work lie in the hypothesis that a single material, Tamarind shells, can play a dual active role: (1) acting as a primary biosorbent for rapid dye capture and (2) serving as a nutrient-rich lignocellulosic substrate that supports growth and stimulates the fungal degradative enzymatic activity. This integration is expected to produce a synergistic effect: initial biosorption protects the fungus from dye toxicity and preconcentrates the substrate, while continuous enzymatic biodegradation regenerates adsorption sites, resulting in a more efficient and robust treatment system.

Therefore, the objective of this study was to develop and evaluate a synergistic system by immobilizing *P. chrysosporium* (Pc) on Tamarind shells (TS) for the removal of the DB71 dye. The synergy was assessed by comparing the integrated system (TS+Pc) with its individual components (TS as a biosorbent and Pc as a biodegradation agent) in batch systems and continuous-flow fixed-bed column reactors.

2. Materials and methods

2.1. Biosorbent preparation and characterization

Tamarind shells (TS) were obtained as waste from the food product industry. TS were crushed and sieved to obtain particles ranging from 500 µm to 1 mm. This fraction was selected on three grounds: it corresponded to the principal yield of the sieving operation; finer fractions were lost during filtration of the batch samples and hindered separation of the solid from the supernatant; and preliminary column trials identified it as giving the most favorable hydrodynamic behavior, since finer material compacted and clogged the bed while coarser material packed less uniformly. The sieved material was washed with deionized water at room temperature (20–23 °C) in approximately three cycles, continuing until the supernatant was colorless, then dried in an oven at 60 °C for 72 h. No chemical modification, carbonization, activation, or solvent extraction was applied at any stage. To confirm that soluble extractives did not interfere with the analytical determination, a blank of TS suspended in deionized water without dye was measured by UV-Vis spectrophotometry at 590 nm; no

absorbance was detected. The TS were then sterilized by autoclaving at 121 °C for 15 min in a single cycle. All TS material used in this study, whether for characterization, batch and column adsorption experiments, or subsequent fungal inoculation, was sterilized in this way. Throughout this work, the term "natural TS" denotes material that has not been chemically modified, carbonized, or activated; it does not imply the absence of sterilization. The sterilized TS was stored in a desiccator and used without further treatment in subsequent experiments. The surface morphology of the material prepared in this way is shown in Figure 1A–B.

The biosorbent was characterized to analyze its surface morphology, identify the functional groups in its structure, and elucidate the adsorption mechanisms of Direct Blue 71 dye (DB71) onto TS. To perform these analyses, scanning electron microscopy (SEM) and Fourier-transform infrared spectroscopy (FTIR) were used. SEM analysis of the TS samples was carried out on a scanning electron microscope (JEOL JSM-6400, JEOL Ltd.) coupled to an EDS probe (Bruker XFLASH 4010). SEM analysis of TS samples was conducted before and after DB71 removal to assess changes in morphology and elemental composition. Also, FTIR analysis of the same biosorbent samples was conducted using a Bruker Tensor 27 FTIR spectrophotometer. Pellets were prepared with KBr, and spectra were recorded over the wavenumber range 400–4000 cm^{-1}. These analyses were performed on the TS samples, both before and after the removal of DB71.

Additionally, the electrokinetic behavior of TS was characterized by microelectrophoresis using a Zeta-Meter System 3+ (Zeta-Meter Inc., USA), following the procedure previously used in our laboratory for lignocellulosic biosorbents [16]. A finely milled subsample of the same TS batch was prepared for this analysis. Suspensions were prepared over the pH range 2.0–12.0, with the pH adjusted using 0.01 M HCl and 0.01 M KOH, and measurements were performed at 25 °C. No background electrolyte was added, so the ionic strength of the suspension varied with pH. Each reported value corresponds to a single determination at the indicated pH.

2.2. Preparation of fungal biomass

The *Phanerochaete chrysosporium* strain was cultured on potato dextrose agar (PDA) in Petri dishes, with 1% bacteriological agar added to enhance solidification. The culture was incubated for 8 days at 30 °C. For all experiments, inocula were obtained by transferring approximately 1 cm^2 of colonized agar from the previously cultured PDA Petri dishes. These samples were taken from the edge of the colony using a cork borer and placed onto new culture medium.

2.3. Immobilization of fungal biomass on Tamarind shells

TS were previously moistened with sterile deionized water to approximately 80% humidity. After moistening and sterilization, 20 g of TS were placed in Petri dishes and inoculated with the *P. chrysosporium* strain as described above. The inoculated shells were incubated at 30 °C in cotton-plugged flasks, which limited evaporative loss while permitting gas exchange, until the hyphae completely invaded the TS; photographs of the material before and after colonization are shown in Figure 6A and B, and an optical micrograph of the hyphal network on the TS surface is shown in Figure 6C. Periodic measurements of colony diameter were recorded at 24-h intervals, and growth curves were generated in triplicate to determine the growth stage at which subsequent experiments would be

conducted.

No nutrient supplementation was provided at any stage; the fungus relied exclusively on the tamarind shell as its carbon source, and the subsequent decolorization experiments were conducted in deionized water containing only the dye.

2.4. Dye removal experiments

DB71 dye removal experiments were conducted to determine the fungal strain's decolorizing capacity in both liquid and solid media. Additionally, DB71 adsorption and removal experiments were performed using the biosorbent (TS) in both batch and continuous systems (fixed-bed columns). In the latter reactor type, the synergistic capacity of the two biological materials to decolorize aqueous solutions containing significant levels of DB71 was also determined. The different system types studied are described below.

2.4.1. DB71 fungal decolorization tests

The decolorization capacity of *Phanerochaete chrysosporium* was evaluated using solid and liquid media. For solid media experiments, PDA and bacteriological agar were used as culture media. The media were supplemented with DB71 at 50 mg/L. After solidification, Petri dishes were inoculated with a 1 cm² plug of *P. chrysosporium* taken from the edge of an actively growing colony on PDA. Plates were incubated at 33–35 °C, and decolorization was monitored visually.

For liquid media experiments, batch cultures were prepared in 125 mL Erlenmeyer flasks containing 100 mL of deionized water supplemented with DB71 at concentrations of 10, 50, and 100 mg/L. Three experimental conditions were evaluated for each dye concentration: (1) a control containing only the dye solution (C), (2) flasks containing the dye solution inoculated with *P. chrysosporium* (C+Pc), and (3) flasks containing the dye solution, 5 g of tamarind shell (TS) as a lignocellulosic substrate, and inoculated with *P. chrysosporium* (C+TS+Pc). Flasks corresponding to conditions (2) and (3) were inoculated with a 1 cm² plug of *P. chrysosporium* and incubated at 33–35 °C without agitation to simulate static conditions; control flasks (condition 1) received no inoculum and were maintained under identical conditions to account for abiotic dye removal. Decolorization was monitored for 24 days by measuring absorbance at 590 nm using a UNICO® S-2150 UV-Vis spectrophotometer. Control flasks without fungal inoculation were maintained under identical conditions to account for abiotic dye removal. All experiments were performed in triplicate as independent experiments, with each replicate set up separately under sterile conditions; reported values are the mean of the three determinations with the corresponding standard deviation.

2.4.2. Batch adsorption experiments with TS

Batch adsorption experiments were conducted to evaluate DB71 removal by tamarind shell (TS) and to determine equilibrium and kinetic parameters. All experiments were performed in triplicate using Erlenmeyer flasks containing 0.1 g of TS and 10 mL of DB71 solution, unless otherwise specified. The mixtures were agitated at 100 rpm on an orbital shaker, and the residual dye concentration was measured by UV-Vis spectrophotometry at 590 nm after appropriate dilution. Adsorption kinetics were

investigated at an initial dye concentration of 10 mg/L, pH 7, and 25 °C, with samples collected at contact times from 5 to 120 min to determine the equilibrium time. The influence of biosorbent dose was evaluated by varying the TS dose from 0.1 to 1.0 g (10–100 g/L), while keeping the initial dye concentration at 10 mg/L and using the previously determined equilibrium time at 25 °C. The effect of pH was studied by adjusting the initial pH of the dye solution (10 mg/L) to values between 3 and 9 using 0.1 M HCl or NaOH, and the experiments were conducted at 25 °C until equilibrium time was reached. Adsorption isotherms were obtained at these three temperatures (25, 35, and 40 °C) using initial DB71 concentrations ranging from 60 to 500 mg/L, with the optimal TS dose (20 g/L) and the pH that yielded the highest removal (pH 3). The mixtures were agitated for 60 min, and the dye concentration at equilibrium was measured. The amount of dye adsorbed per gram of TS at equilibrium, q_e (mg/g), was calculated using the following mass balance equation:

$$qt = \frac{(C_o - C_t)V}{m} \quad (1)$$

Where C_o is the initial concentration of DB71 in the supernatant, C_t is the concentration of DB71 in the supernatant at time *t, V* is the volume of solution (L), *m* is the mass of the biosorbent (g), and *qt* is the dye concentration in the biosorbent (mg/g). Kinetic and isotherm adsorption data were fitted by nonlinear regression to the corresponding models, using Statistica v7.0. Both the Levenberg–Marquardt and Quasi-Newton estimation algorithms were applied to each model and the results compared; differences between them were minor, and the better-converging solution was retained. The convergence criterion was 1×10^{-4}. Initial parameter values were set close to experimentally observed quantities where available, such as *q*e for the kinetic models and Q_0 for the Langmuir isotherm, and were varied in several cases to verify that convergence did not depend on the starting values.

2.4.3. Fixed-bed column adsorption experiments

Fixed-bed column experiments were conducted to evaluate the continuous removal of DB71 using tamarind shell (TS) alone and TS inoculated with *Phanerochaete chrysosporium* (TS+Pc). The columns were constructed from plexiglass tubes with an internal diameter of 4 cm and a bed height of 15 cm. TS particles ranging from 500 μm to 1 mm were dry-packed into the columns in layers, with tapping between successive additions to promote uniform packing, and supported on a glass wool plug. This gave a packed mass of 94.6 g for the TS column and 103 g for the TS+*Pc* column, corresponding to bulk densities of 0.50 and 0.55 g/cm³, respectively. The beds were not pre-wetted before operation, and bed porosity and liquid holdup were not determined. The influent was maintained at pH 7 in both columns; this value was selected for compatibility with *P. chrysosporium* rather than optimal biosorption, since batch experiments identified pH 3 as optimal, and it was applied to both configurations to keep them directly comparable. The reservoir was held at 35 °C with an immersion heater, and the column was insulated to retain heat during operation; the column itself was not independently thermostatted. No clogging, compaction, or loss of flow was observed in either configuration, and no backwashing was performed. For the TS+Pc columns, TS was previously sterilized, moistened to a substrate moisture content of approximately 80% on a wet basis (g water per g moist material), determined gravimetrically, and inoculated with *P. chrysosporium*, as described above; photographs of the material before and after fungal colonization are shown in Figure 6. The

packed columns were then connected to a reservoir containing a DB71 solution at an initial concentration of 10 mg/L, with a pH of 7. The solution was fed downward through the column by gravity at a constant flow rate of 1 mL/min, regulated by a stopcock. A water heater was placed in the reservoir to maintain the solution temperature at 35 °C. Effluent samples were collected at regular intervals: every 5 min during the first hour of operation and every 20 min thereafter until the column reached saturation, for a total operating time of up to 3 h. The dye concentration in the effluent was measured by UV-Vis spectrophotometry at 590 nm. Breakthrough curves were constructed by plotting the ratio of effluent to influent concentration (C/C_0) as a function of time, and the breakthrough point was defined as the time at which C/C_0 reached 0.5. Each column configuration was operated once; the breakthrough experiments were not replicated. The experimental breakthrough data were fitted to the Thomas, Yoon–Nelson, and dose-response models to evaluate the columns' dynamic behavior.

3. Results and discussion

3.1. Scanning electron microscopy (SEM) analysis

The surface morphology and elemental composition of tamarind shell (TS) before and after DB71 adsorption were examined by scanning electron microscopy coupled with energy-dispersive X-ray spectroscopy (SEM-EDS). Figure 1 presents micrographs of natural TS at two magnifications (Figure 1A: 100×, Figure 1B: 1000×) and DB71-loaded TS at three magnifications (Figure 1C: 500×, Figure 1D: 2000×, Figure 1E: 5000×).

The natural TS exhibited a rough, alveolar-like surface morphology with visible porosity on the sides (Figures 1A and B). This highly irregular and porous texture likely results from milling, which exposes the internal lignocellulosic structure. The numerous pores and crevices favor adsorption by increasing available surface area and providing multiple potential binding sites for dye molecules. Similar rough, porous surface morphologies have been reported for other agricultural waste-based biosorbents, including wheat shells, orange peel, and *Robinia pseudoacacia* fibers, all of which demonstrated effective dye-removal capacities [17–19]. After the biosorption process (Figure 1C–E), no dramatic changes in overall surface morphology were observed, indicating that DB71 adsorption did not alter the structural integrity of the TS. However, some pores appear partially filled or coated, suggesting that dye has deposited on the surface. Comparable observations have been reported in a study on the adsorption of Congo Red onto modified peanut husks [20], in which post-adsorption micrographs revealed pore filling without significant surface degradation.

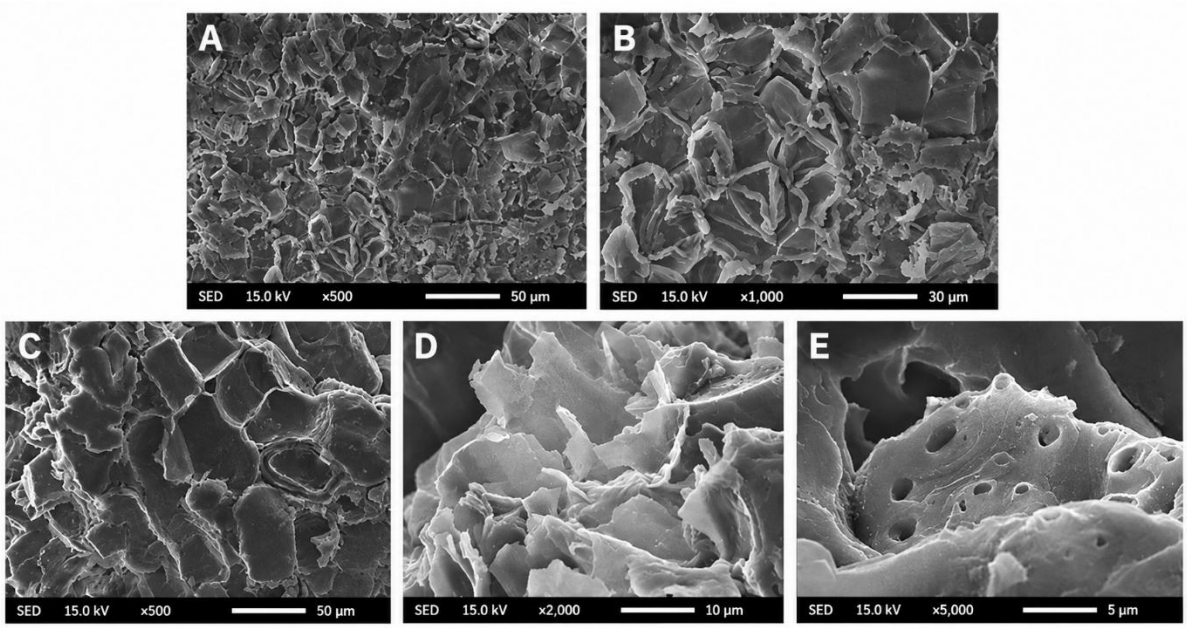


Figure 1. SEM micrographs of tamarind shell (TS) before and after DB71 biosorption. (A) Natural TS at 500×. (B) Natural TS at 1000×. (C) DB71-loaded TS at 500×. (D) DB71-loaded TS at 2000×. (E) DB71-loaded TS at 5000×.

Additionally, Figure 2 shows the elemental distribution map of natural TS. The predominant elements were carbon (60.54%), oxygen (31.23%), nitrogen (6.5%), and calcium (0.7%), with minor amounts of potassium, magnesium, and aluminum. This composition is consistent with the lignocellulosic nature of TS, which is rich in carbohydrates and proteins. Similar elemental compositions, characterized by high carbon and oxygen contents, have been reported for various lignocellulosic biomasses, including sorghum agricultural waste and sugarcane bagasse–based biosorbents [21]. The presence of nitrogen suggests proteinaceous material, while calcium and other metals are typical of plant biomass and have been identified in other agricultural residues used as biosorbents.

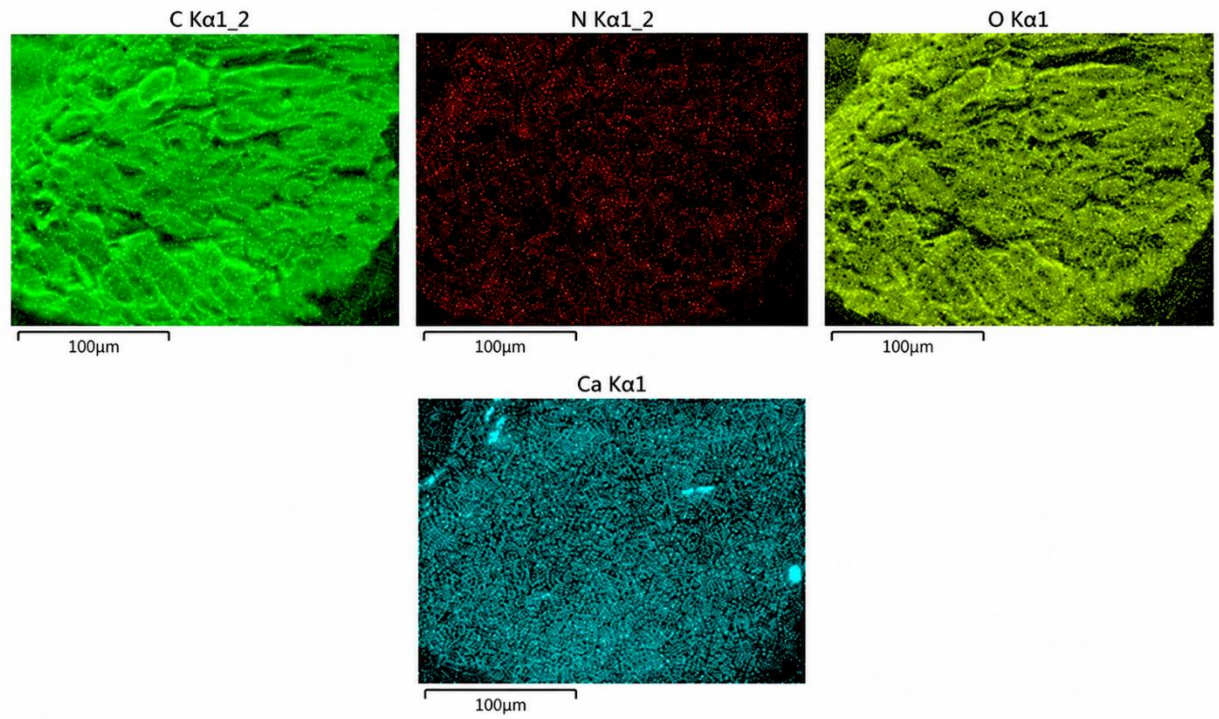


Figure 2. EDS elemental distribution map of natural tamarind shell (TS) showing the relative abundance of carbon, oxygen, nitrogen, calcium, and trace elements.

After biosorption, EDS analysis (Figure 3A) revealed additional elements. Sulfur (purple) and sodium (not shown in the map but confirmed by the spectrum) were detected on the DB71-loaded TS surface. These elements are characteristic of the DB71 molecule, which contains four sulfonate groups (–SO_3Na). The detection of sulfur provides direct evidence of dye binding: sulfur is absent from natural TS and, because the experimental system comprises only deionized water, DB71, and HCl and NaOH for pH adjustment, the dye is the only possible source. Sodium was likewise detected and is consistent with dye uptake, but it is not diagnostic, since NaOH used for pH adjustment constitutes a second possible source. The detection of such marker elements (e.g., sulfur from sulfonate groups) has been used in other studies to confirm the successful uptake of anionic azo dyes onto biosorbents [22]. The corresponding EDS spectrum (Figure 3B) confirmed the signals for sulfur and sodium, along with the expected carbon, oxygen, nitrogen, and calcium. A small gold peak was also observed, which originates from the conductive coating applied to the samples before analysis. The pore filling observed by SEM could, in principle, reflect deposition of species other than the dye. This is excluded by the elemental evidence: a precipitating sodium salt would contribute sodium, but not sulfur, and no sulfate is present in the system. Precipitation is not thermodynamically accessible, since the sodium released by the dye reaches at most 1.63 mM at the highest initial concentration examined, about three orders of magnitude below the saturation of any relevant sodium salt. These results collectively confirm that DB71 was successfully retained on the TS surface via biosorption. The elemental composition of TS is also similar to that of other plant-based materials, with carbon and oxygen being the major constituents, followed by nitrogen and trace metals [21]. The detection of sulfur and sodium on the dye-loaded TS is consistent with findings from other studies on the adsorption of sulfonated azo dyes onto lignocellulosic substrates, where the presence of these elements is used as a marker for successful dye uptake [6]. Overall, the SEM-EDS analysis confirms that TS possesses suitable morphological and

chemical characteristics for the removal of DB71 from aqueous solutions.

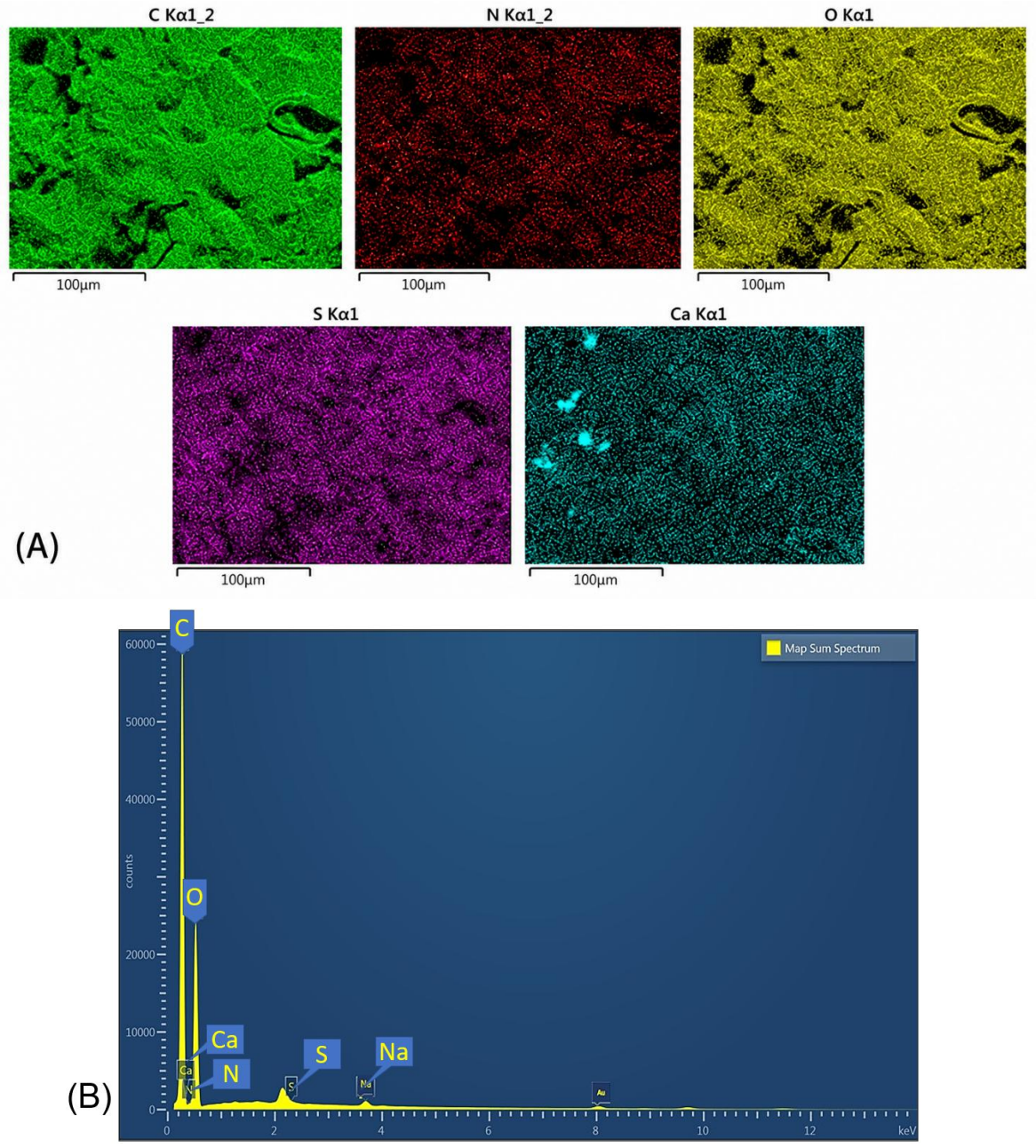


Figure 3. EDS analysis of DB71-loaded tamarind shell (TS). (A) Elemental distribution map showing the spatial distribution of detected elements. (B) EDS spectrum confirming the presence of sulfur and sodium as marker elements of DB71 uptake.

3.2. FTIR analyses

Fourier-transform infrared spectroscopy (FTIR) was employed to identify the main functional groups on the tamarind shell (TS) surface before and after DB71 adsorption and to elucidate the possible binding mechanisms involved in dye removal. Figure 4 shows the FTIR spectra of natural TS and DB71-loaded TS in the wavenumber range of 400–4000 cm^{-1}. The natural TS spectrum showed a

broad, intense band between 3746 and 3400 cm^{-1} (Figure 4), attributed to O–H stretching vibrations of hydroxyl groups in cellulose, hemicellulose, and lignin, as well as adsorbed water. The bands at 2924 and 2848 cm^{-1} correspond to asymmetric and symmetric C–H stretching of methyl and methylene groups, indicating the presence of aliphatic structures typical of lignocellulosic materials [21]. The region between 1765 and 1615 cm^{-1} displayed several bands: a sharp peak at 1733 cm^{-1} is characteristic of C=O stretching from carbonyl groups of carboxylic acids, aldehydes, or esters present in hemicellulose and lignin [23]; the bands at 1691 and 1657 cm^{-1} correspond to C=C stretching of aromatic rings and amide I (N–C=O) vibrations, respectively, suggesting the presence of lignin and proteinaceous components [24]; the bands at 1553 and 1525 cm^{-1} correspond to aromatic skeletal vibrations of the lignin fraction, while those at 1385 and 1337 cm^{-1} are attributed to C–H bending in cellulose and hemicellulose [23–25]. Finally, the strong absorption band around 1065–1057 cm^{-1} is typical of C–O stretching vibrations in polysaccharides (cellulose and hemicellulose) [25].

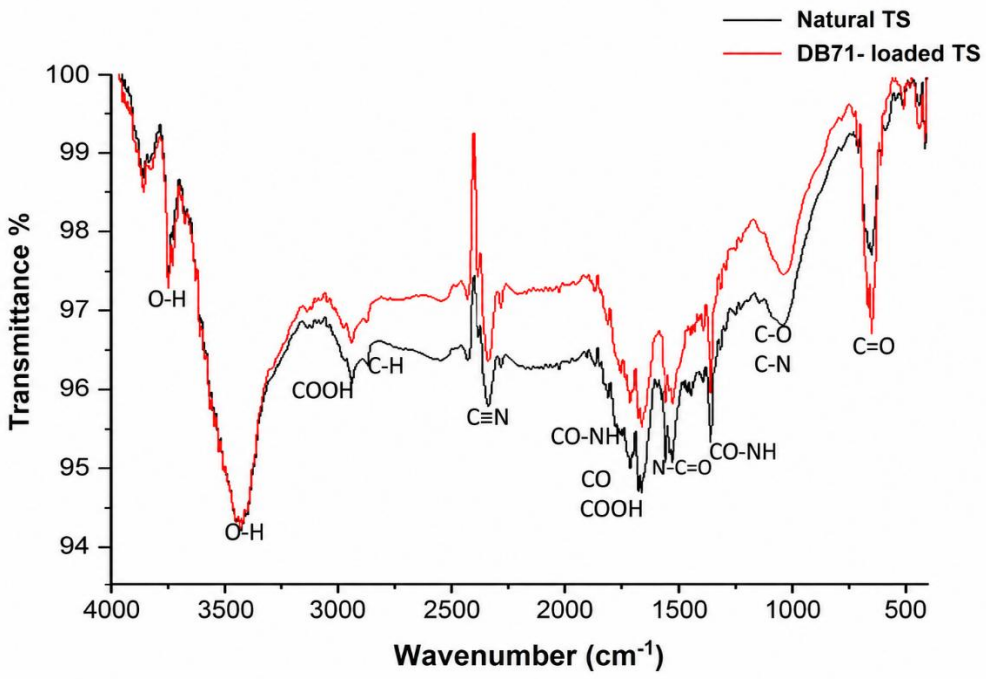


Figure 4. FTIR spectra of natural tamarind shell (TS, black line) and DB71-loaded tamarind shell (TS-DB71, red line) in the wavenumber range of 400–4000 cm^{-1}.

After DB71 adsorption, the FTIR spectrum of TS showed notable changes in the intensity and position of some characteristic bands. The O–H stretching band broadened and shifted slightly, suggesting possible hydrogen-bonding interactions between the dye and the hydroxyl groups of the TS surface. The carbonyl and amide bands in the 1700–1600 cm^{-1} region exhibited reduced intensity, suggesting that carboxyl and amino groups are involved in binding to DB71. Similar behavior has been reported for the adsorption of anionic azo dyes onto lignocellulosic biosorbents, in which electrostatic interactions and hydrogen bonding between the dye's sulfonate groups and the biomass's carboxyl and hydroxyl groups are the primary binding mechanisms [26]. Importantly, the aliphatic C–H stretching bands at 2924 and 2848 cm^{-1} also showed a decrease in intensity after dye adsorption. This reduction

may be attributed to conformational changes in the cellulose and hemicellulose chains upon interaction with the dye molecules or to the coverage of these hydrophobic regions by the adsorbed DB71, which contains aromatic rings and sulfonate groups. Similar decreases in aliphatic C–H band intensities have been observed in other studies on the adsorption of organic contaminants onto lignocellulosic materials, where the interaction was attributed to hydrophobic and van der Waals forces between the aliphatic chains of the biosorbent and the aromatic moieties of the adsorbate [27].

Similar spectral changes in this region have been reported in studies of organic dye adsorption onto carbon-based adsorbents, where the interactions were attributed to weak noncovalent forces, such as van der Waals interactions and hydrogen bonding involving carbonyl and aliphatic moieties [28]. In summary, the FTIR results confirm that TS is rich in functional groups such as hydroxyls, carboxyls, carbonyls, and amines, which are typical of lignocellulosic materials and serve as active binding sites for various substances. These groups are consistent with TS's chemical composition, which is primarily cellulose, hemicellulose, and lignin. The observed spectral changes after DB71 adsorption provide evidence that these functional groups participated in dye retention, likely through electrostatic attraction, hydrogen bonding, and possibly π–π interactions between the dye's aromatic rings and the lignin backbone.

3.3. Fungal immobilization and growth on tamarind shell

The ability of *Phanerochaete chrysosporium* to colonize and grow on tamarind shell (TS) as a solid support and carbon source was evaluated. Figure 5 shows the growth curve of *P. chrysosporium* on TS, expressed as colony diameter over time. After inoculation, a short lag phase (approximately 24 h) was observed, followed by an exponential growth phase from day 1 to day 6, during which the mycelium rapidly expanded across the TS surface. The fungus reached the stationary phase on day 7, having completely colonized the surface of the TS (9-cm-diameter Petri dish).

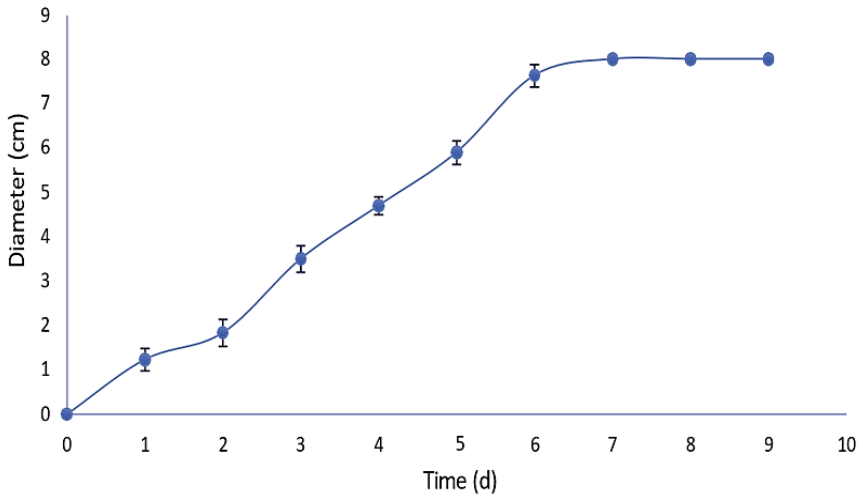


Figure 5. Growth curve of *Phanerochaete chrysosporium* on tamarind shell (TS), expressed as colony diameter (cm) over time (days). Error bars represent the standard deviation from triplicate experiments.

Figures 6A and B show photographs of Petri dishes illustrating the progressive colonization of TS by *P. chrysosporium*, from initial inoculation to full coverage. Figure 6C shows an optical microscopy image (40× magnification) of *P. chrysosporium* hyphae growing on the TS surface, revealing the characteristic branching mycelial network associated with the biosorbent particles. These results demonstrate that TS is not only a biosorbent but also an effective lignocellulosic substrate for *P. chrysosporium*. The rapid growth and complete colonization within 6–7 days suggest that TS provides readily accessible nutrients, likely including residual sugars and polysaccharides (cellulose, hemicellulose) that the fungus can metabolize [29]. The observed growth rate is comparable to or faster than that reported for other lignocellulosic residues, such as mulberry stalks (9 days for full colonization) and wheat straw (8–12 days) [30,31]. The relatively rapid colonization may be attributed to the porous, rough surface morphology of TS (as shown in Figure 1), which facilitates hyphal attachment and penetration, and to the absence of growth inhibitors commonly found in some seeds or unprocessed plant materials, such as phenolic allelochemicals that suppress microbial growth and colonization [32]. The successful immobilization of *P. chrysosporium* on TS yields a dual-function material: TS serves as a physical support and biosorbent. At the same time, the fungal biomass provides enzymatic degradation capacity for dye removal in subsequent experiments.

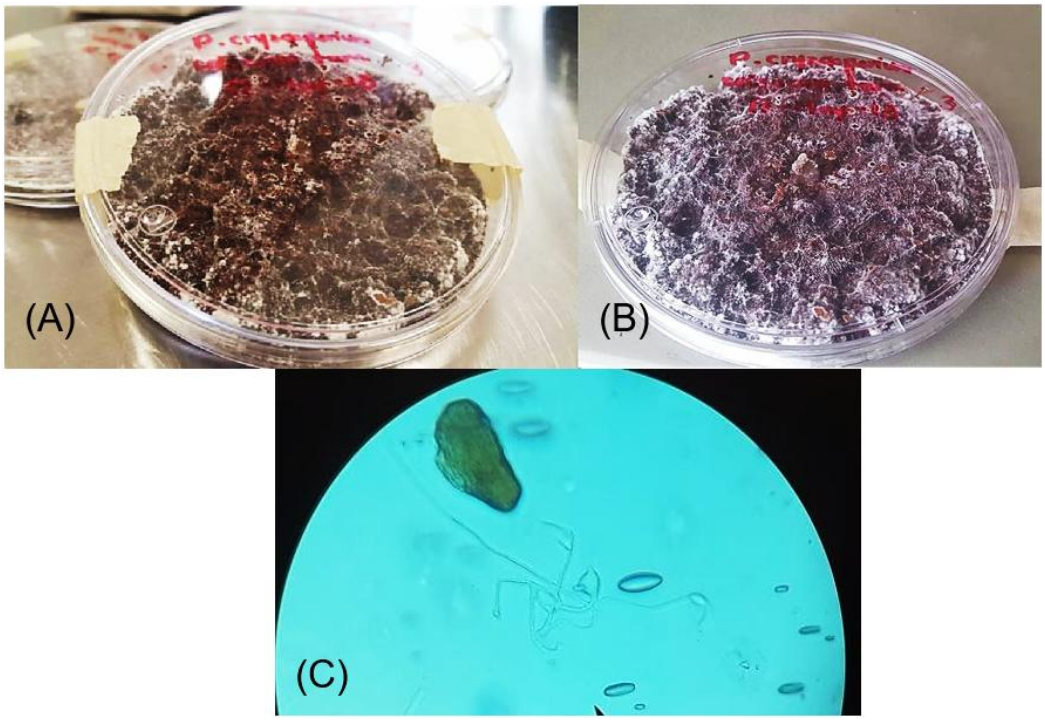


Figure 6. Colonization of tamarind shell (TS) by *Phanerochaete chrysosporium*. (A, B) Photographs showing progressive mycelial coverage of TS in Petri dishes from inoculation to full colonization. (C) Optical microscopy image (40×) showing hyphal networks attached to and penetrating TS particles.

3.4. Decolorization of DB71 by Phanerochaete chrysosporium*: Solid and liquid media tests*

The decolorization capacity of *Phanerochaete chrysosporium* was first evaluated on solid media. Figure 7 shows the decolorization of DB71 (50 mg/L) on two different culture media. On PDA medium (Figure 7A), the fungus exhibited initial mycelial growth that covered the plate within 6 days, followed by progressive decolorization of the surrounding medium. This behavior indicates that, in the presence of easily metabolizable carbon sources from PDA, the fungus prioritizes growth and subsequently secretes ligninolytic enzymes that degrade the dye. In contrast, on bacteriological agar without added nutrients (Figure 7B), *P. chrysosporium* did not exhibit visible mycelial expansion; however, the dye was completely decolorized within 72 h of inoculation. This result suggests that under nutrient-limited conditions, the fungus activates a stress response, likely producing extracellular enzymes (such as lignin peroxidase or manganese peroxidase) to scavenge carbon or energy from the recalcitrant dye molecules, despite the absence of visible growth. Similar observations have been reported for other white-rot fungi, in which starvation conditions triggered higher ligninolytic enzyme activities [33]. The maximum DB71 concentration that *P. chrysosporium* could completely decolorize on a nutrient-free solid medium was 300 mg/L (data not shown), indicating remarkable tolerance and degradation capacity.

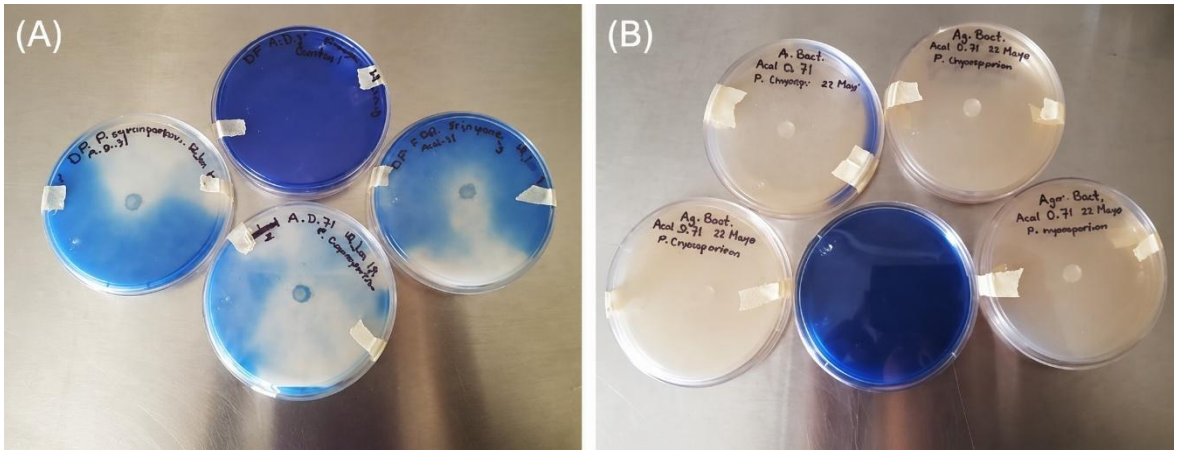


Figure 7. Decolorization of DB71 (50 mg/L) by *Phanerochaete chrysosporium* on solid media. (A) Potato dextrose agar (PDA) after 6 days of incubation. (B) Bacteriological agar without added nutrients after 72 h of inoculation.

Liquid batch experiments were conducted at initial DB71 concentrations of 10, 50, and 100 mg/L under three experimental conditions: dye alone (control, C), dye with fungus (C+Pc), and dye with fungus and tamarind shell as a lignocellulosic substrate (C+TS+Pc). Figure 8 presents the decolorization kinetics at 10 mg/L. The control showed negligible dye removal throughout the 24-day incubation period, confirming that abiotic processes were not significant. The C+Pc system removed approximately 68% of the dye, whereas the C+TS+Pc system achieved 98% decolorization. Notably, in the C+TS+Pc system, removal reached about 60% by day 9, whereas the C+Pc system removed only 20%. This enhanced performance is attributed to the combined effects of TS biosorption (as previously discussed) and fungal enzymatic degradation stimulated by the lignocellulosic substrate.

The rapid initial removal is consistent with dye uptake onto both the TS surface and the fungal mycelium. The final extent of removal, however, exceeds what biosorption onto TS alone can account for. The liquid-phase experiments employed 5 g of TS in 100 mL, a dose of 50 g/L, which lies within the range examined in the dose-optimization experiments; at that dose and at the same initial dye concentration, TS in the absence of the fungus removed approximately 50% of the DB71, and removal did not exceed 58% at any dose between 10 and 100 g/L. Compared with 98% for the combined system, at least a third of the removal observed here arises from a process other than biosorption onto TS. We note that the two experiments differ in pH, agitation, and contact time, so this comparison bounds rather than quantifies the adsorptive contribution. As observed visually, the blue color in the TS biomass gradually disappeared by the end of the treatment. Similar synergistic effects have been reported for *P. chrysosporium* immobilized on other lignocellulosic supports, such as wheat straw and corncobs, for decolorizing azo dyes [34].

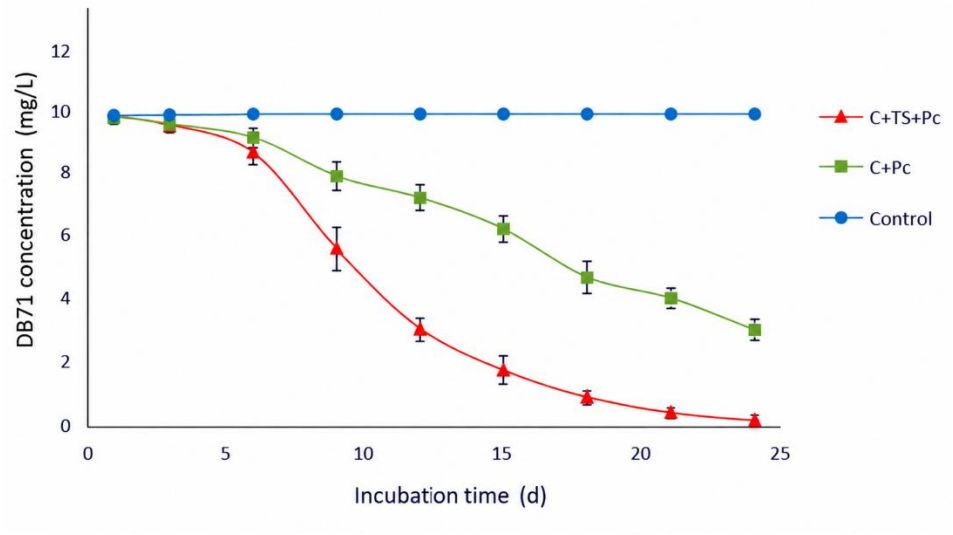


Figure 8. Decolorization kinetics of DB71 at 10 mg/L by *Phanerochaete chrysosporium* under three experimental conditions: dye alone (C, control), dye with fungus (C+Pc), and dye with fungus and tamarind shell as lignocellulosic substrate (C+TS+Pc).

Additionally, Figure 9 shows the results for an initial DB71 concentration of 50 mg/L. The C+Pc system removed 49% of the dye after 24 days, while the C+TS+Pc system achieved 76% removal. The difference between the two systems was less pronounced than at 10 mg/L, suggesting that the higher dye concentration partially inhibited fungal growth or enzyme activity. Nevertheless, the presence of TS as a carbon source still provided a clear benefit, likely by sustaining higher fungal biomass and inducing greater enzyme production. At the highest concentration tested (100 mg/L; Figure 10), the C+Pc system removed only 16% of DB71, indicating strong inhibition. In contrast, the C+TS+Pc system removed 67% of the dye, demonstrating that the lignocellulosic substrate significantly alleviated toxicity and enabled substantial decolorization even at relatively high dye loads. The control flasks (dye alone, without fungus) showed no significant change in concentration over time, confirming that the observed removal was biological. Throughout all liquid-batch experiments, initial dye uptake onto the fungal biomass and TS was visually evident, and the blue color on the biomass

diminished over the course of the treatment. This observation is reported for completeness but is not interpreted mechanistically, since loss of color from the biomass is equally consistent with desorption, with transformation into colorless products, and with enzymatic degradation. The present design does not allow quantitative separation of the adsorptive and degradative contributions to the removal observed in the combined system. The superior performance of the C+TS+Pc system across all concentrations underscores the importance of providing a lignocellulosic support that both immobilizes the fungus and induces ligninolytic enzymes. This dual-function approach offers a promising strategy for treating textile wastewater containing moderate-to-high concentrations of azo dyes.

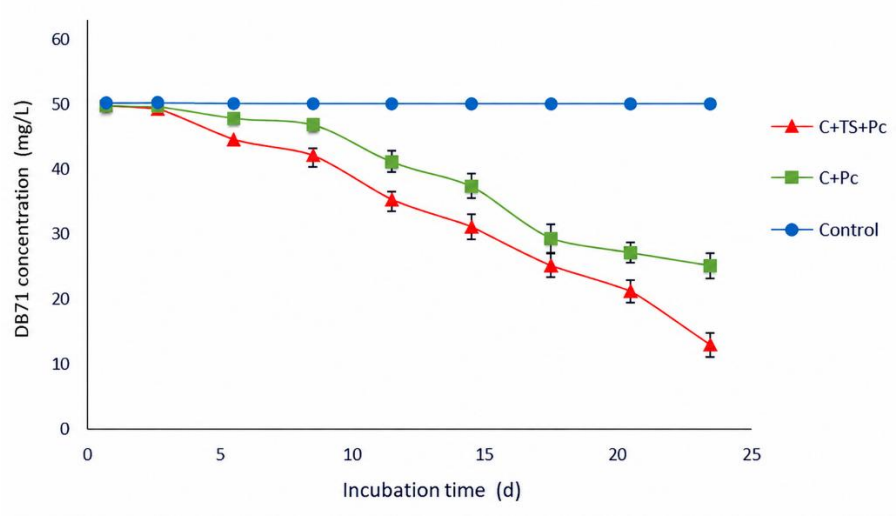


Figure 9. Decolorization kinetics of DB71 at 50 mg/L by *Phanerochaete chrysosporium* under three experimental conditions: dye alone (C, control), dye with fungus (C+Pc), and dye with fungus and tamarind shell (C+TS+Pc).

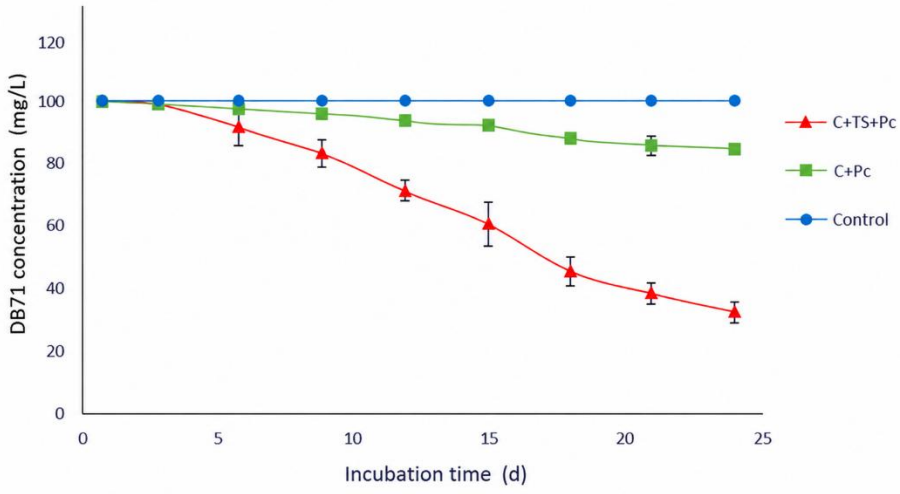


Figure 10. Decolorization kinetics of DB71 at 100 mg/L by *Phanerochaete chrysosporium* under three experimental conditions: dye alone (C, control), dye with fungus (C+Pc), and dye with fungus and tamarind shell (C+TS+Pc).

3.5. Biosorption kinetics of DB71 onto tamarind shell

The biosorption kinetics of DB71 onto tamarind shell (TS) were investigated at an initial dye concentration of 10 mg/L, pH 7, and 25 °C, with samples withdrawn at contact times of up to 120 min (Figure 11). Uptake was markedly fast: approximately 46% of DB71 was removed within the first 5 min of contact, after which removal efficiency rose only marginally and plateaued at about 52%–53% by 60 min, which was taken as the equilibrium time. Expressed as the amount adsorbed per unit mass of biosorbent, this plateau corresponds to an equilibrium uptake of $q_e \approx 0.52$ mg/g (for $C_0 = 10$ mg/L and a biosorbent dose of 10 g/L). The very rapid initial uptake reflects the large number of unoccupied, readily accessible binding sites on the TS surface at the start of the experiment, as well as the steep concentration gradient between the bulk solution and the sorbent surface. As these sites became progressively occupied and the gradient relaxed, the net uptake rate declined until equilibrium was reached. This biphasic profile, a rapid initial step followed by a slow approach to a plateau, is characteristic of dye biosorption onto lignocellulosic materials and has been reported for the removal of DB71 using other agricultural by-products, such as wheat shells [19,35].

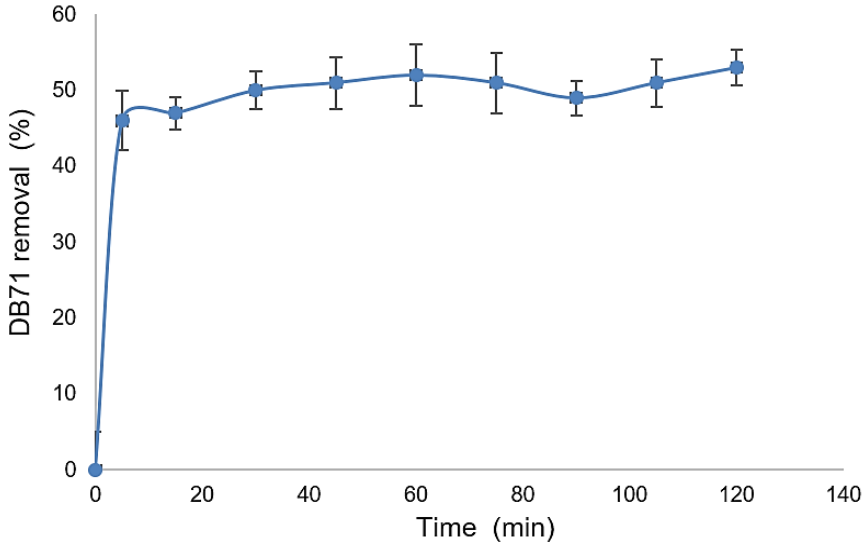


Figure 11. DB71 biosorption kinetics onto TS as a function of contact time ($[DB71]_0 = 10$ mg/L; biosorbent dose = 10 g/L; pH 7; temperature = 25 °C). Error bars represent the standard deviation from triplicate experiments.

To elucidate the rate-controlling mechanism, the experimental kinetic data were fitted to three nonlinear models: pseudo-first-order, pseudo-second-order, and Elovich [36–38]. Table 1 summarizes the estimated kinetic parameters and their corresponding correlation coefficients (R). Figure S1 shows plots of the model fit to the experimental data. All three models reproduced the overall kinetic profile well ($R > 0.99$), with the pseudo-second-order equation providing the closest fit ($R = 0.9968$). Its equilibrium capacity, $q_e = 0.51$ mg/g, agrees closely with the experimental value (~0.52 mg/g), and the associated initial sorption rate, $h_0 = k_2 q_e^2 = 0.76$ mg/g min, quantifies the steep early uptake evident in Figure 11. The pseudo-second-order equation was originally derived assuming that the rate-limiting step involves electron sharing or exchange between the adsorbate and the biosorbent surface,

characteristic of chemisorption [36]; this reflects the model's derivation, not an inference drawn from its fit quality. However, the differences in fit quality among the three models are small, and the models are statistically near-equivalent over the present data set; the close fit of the pseudo-second-order equation cannot, on its own, be taken as proof of a particular sorption mechanism. As emphasized in recent critical assessments of adsorption kinetics, an excellent pseudo-second-order fit is a common—and often unavoidable—mathematical outcome for systems that equilibrate rapidly, and it does not by itself establish that chemisorption is the rate-controlling step [39,40]. The mechanistic interpretation of the DB71–TS system is therefore grounded primarily in the complementary spectroscopic, pH, and equilibrium evidence rather than in the kinetic model ranking alone.

Table 1. Kinetic model parameters and correlation coefficients (R)* for DB71 biosorption onto tamarind shell (TS).

Biosorbent	Kinetic model		
	Pseudo-first-order	Pseudo-second-order	Elovich
Tamarind shells (TS)	K_L= 0.4791 min^{-1} q_e = 0.5051 mg/g R = 0.9948	K_2 = 2.893 g/mg min q_e = 0.5136 mg/g R = 0.9968	α = 1.71×10^8 mg/g min β= 53.40 g/mg R = 0.9955

* Correlation coefficients were calculated including the origin (t = 0, qt = 0) through which all three models pass by construction.

The pseudo-first-order model also described the data well (R = 0.9948), with q_e = 0.51 mg/g and a rate constant K_L = 0.48 min^{-1}. A K_L of this magnitude indicates that the process is essentially complete within the first 15–20 min, consistent with the experimental curve, and that external mass transfer and the rapid occupation of surface sites govern the early stage of uptake.

Additionally, the Elovich model also fitted the data well (R = 0.9955). In this model, α is the initial adsorption rate, and β is related to the extent of surface coverage and the sorption activation energy. The fitted α (of the order of 10^8 mg/g min) is extraordinarily large and must be interpreted with caution: it is a mathematical consequence of the near-instantaneous initial uptake (most of the equilibrium capacity was attained within the first 5 min) combined with the limited time resolution of the early sampling, rather than a physically transferable rate constant. The magnitude of α is consistent with the class of kinetic behavior to which this system belongs. Wu et al. defined the approaching-equilibrium parameter $R_E = 1/(q_{ref}\cdot\beta)$ and, surveying 64 adsorption systems, assigned 80% to a "mild rising" zone (R_E = 0.1–0.3) and the remainder to a rapid-adsorption zone [41]. Here, R_E = 0.036, placing DB71–TS in the latter. For comparison, α values between 0.0205 and 2.71 mg/g·min have been reported for metal biosorption onto guava seed under comparable batch conditions [16]. Two features of the present dataset limit what α can represent. The first sample, at 5 min, already corresponds to 88% of the equilibrium uptake, so the rising portion of the curve is unsampled, and the fitted equation predicts half-uptake at approximately 7 ms—four orders of magnitude below the shortest observed time. Furthermore, since qt depends on ln(α), an uncertainty of ±0.05 mg/g in the 5-min point corresponds to a factor of 14 in α. The fitted value is therefore constrained only to within one or two orders of magnitude and is reported here as an empirical constant without mechanistic interpretation. The same limitation applies to discrimination among the kinetic models. At 5 min, the first measured

point, the three fitted equations agree to within 0.007 mg/g; at 1 min, they span 0.19 to 0.43 mg/g, and at 0.1 min, they differ by a factor of sixteen (Figure S1, inset). The models are therefore indistinguishable over the measured interval and maximally divergent over the unmeasured interval, which further shows that the ranking of their fit statistics carries no mechanistic weight. In the Elovich framework, α represents the initial adsorption rate. At the same time, β (g/mg) inversely relates to the slope of qt versus ln t, indicating how the adsorption rate decays as the surface fills. A fitted β of approximately 53 g/mg suggests a shallow qt–ln t relationship, with only a marginal increase in uptake after an initial rapid phase, consistent with observed saturation. Both α and β are empirical values influenced by qt units and solid–liquid ratios, making them non-comparable across different conditions. Additionally, as kinetics were measured at a single temperature, no activation energy can be derived from β. These constants are sensitive to early sampling-time resolution and serve as qualitative descriptors of initial interactions rather than universal physical constants [42,43].

Overall, the kinetic results show that DB71 biosorption onto TS is rapid, reaching equilibrium within about 60 min, and is well represented by the pseudo-second-order and, comparably, the pseudo-first-order and Elovich equations. The short equilibration time is advantageous for practical batch operation. Because the three models are nearly indistinguishable in goodness of fit, the rate-limiting step is not determined solely by the kinetic models; the nature of the DB71–TS interaction is examined further in light of the equilibrium isotherms and thermodynamic parameters.

3.6. Effect of biosorbent dose

The effect of biosorbent dose on DB71 removal was evaluated by varying the TS concentration from 10 to 100 g/L at 25 °C, with an equilibrium contact time of 60 min, as established above. Figure 12 presents the results. Contrary to the commonly expected monotonic increase in removal efficiency with increasing biosorbent dose, the results revealed a nonlinear relationship between dose and removal percentage. The maximum removal of approximately 58% was achieved at 20 g/L, which was therefore identified as the optimal biosorbent dose and used in all subsequent batch experiments. At doses below 20 g/L, removal efficiency was lower, consistent with fewer available binding sites relative to the dye concentration in solution. However, beyond the optimal dose of 20 g/L, removal efficiency did not continue to increase; instead, it slightly declined as the dose increased toward 100 g/L. This behavior has been reported for other lignocellulosic biosorbents and is generally attributed to particle aggregation at high biosorbent concentrations: as the mass of TS increases in a fixed volume of solution, particles tend to cluster and form agglomerates, which effectively shield internal and surface active sites from contact with the dye molecules, thereby reducing the overall adsorption efficiency per unit mass of biosorbent [44,45]. Additionally, at high biosorbent doses with a fixed, relatively low initial dye concentration (10 mg/L), the ratio of available binding sites to dye molecules becomes very large, indicating that the biosorbent is far from saturation and that the incremental contribution of additional material diminishes. This effect, often described as a decrease in removal value at higher doses due to saturation of adsorption sites, is well documented in batch biosorption studies using agricultural waste materials [7,35]. It should also be noted that the uptake per unit mass in these experiments is constrained by the mass balance rather than by the affinity of the biosorbent: at an initial concentration of 10 mg/L and a dose of 20 g/L, complete removal would correspond to q_e = 0.5 mg/g. The values reported in this section therefore quantify removal efficiency and should not

be read as capacities; the uptake capacity of TS, determined from the equilibrium isotherms at the same dose, is 15.45–18.11 mg/g over the range 25–40 °C (Section 3.6).

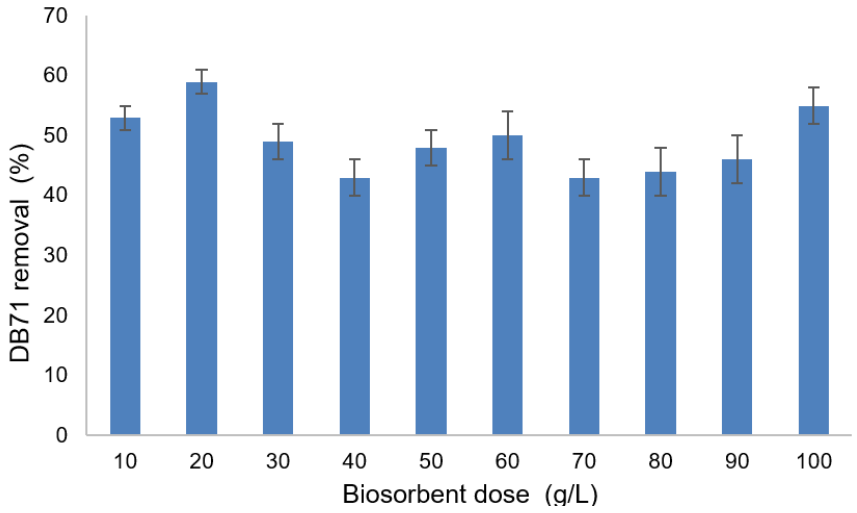


Figure 12. Effect of biosorbent dose on DB71 removal by TS ([DB71]$_0$ = 10 mg/L; pH 7; contact time = 60 min; temperature = 25 °C). Error bars represent the standard deviation from triplicate experiments.

It is also worth noting that the differences in removal efficiency across the tested dose range were relatively modest—with most doses yielding removal values between approximately 45% and 58%—suggesting that TS has a moderate but consistent affinity for DB71 across a broad range of solid-to-liquid ratios. This moderate efficiency is consistent with the intrinsic surface chemistry of natural, unmodified TS, which, while rich in functional groups as established by FTIR spectra, has not undergone any chemical activation or surface treatment. The identification of 20 g/L as the optimal dose balances removal performance against biosorbent consumption at the concentration examined. The material efficiency of this condition depends strongly on the dye load: at 10 mg/L, the dose corresponds to approximately 3.4 g of TS per mg of DB71 removed, whereas at the concentrations used for the equilibrium isotherms, the same dose removes some 360 mg/L of dye, or 0.055 g of TS per mg. Since textile effluents typically contain dye at tens to hundreds of mg/L, the practical material requirement is considerably lower than the dose-optimization experiment alone would indicate. Compared with functionalized and nanostructured sorbents, unmodified TS offers moderate capacity per unit mass; its advantages lie in its cost, its availability as an agro-industrial residue, and its dual function as a lignocellulosic substrate for *P. chrysosporium*, rather than in capacity per gram.

3.7. Influence of solution pH on DB71 biosorption by TS

Solution pH is one of the most influential variables in biosorption, as it governs the protonation state of functional groups on the biosorbent surface and, in turn, the balance of electrostatic and non-electrostatic interactions available for dye binding. In the present system, this effect is dominated by the surface chemistry of the lignocellulosic TS rather than by the dye itself: the four sulfonate groups of DB71 are strongly acidic and remain deprotonated, so the molecule stays anionic across the entire

pH range examined, and the observed variation in removal reflects changes at the biosorbent surface. The influence of initial pH on DB71 removal by TS was evaluated over pH 3 to 9, with a fixed initial dye concentration of 10 mg/L, a biosorbent dose of 20 g/L, a temperature of 25 °C, and an equilibrium contact time of 60 min (Figure 13). Removal efficiency increased progressively as the solution pH decreased, reaching a maximum of approximately 69% at pH 3 and declining markedly toward neutral and alkaline values. This trend can be rationalized through the acid–base chemistry of the surface groups identified by FTIR. At low pH, the high concentration of H^+ ions protonates the weakly acidic carboxyl (–COOH) and hydroxyl (–OH) groups and any amino groups present ($–NH_2 \rightarrow –NH_3^+$), suppressing the negative charge that would otherwise develop on the surface and creating locally protonated, positively charged sites. Under these conditions, electrostatic repulsion toward the anionic dye is minimized, while attractive contributions—electrostatic attraction at protonated amino sites, together with hydrogen bonding and π–π interactions involving the aromatic rings of DB71 and the lignin fraction of TS—become favorable, accounting for the high removal observed at pH 3.

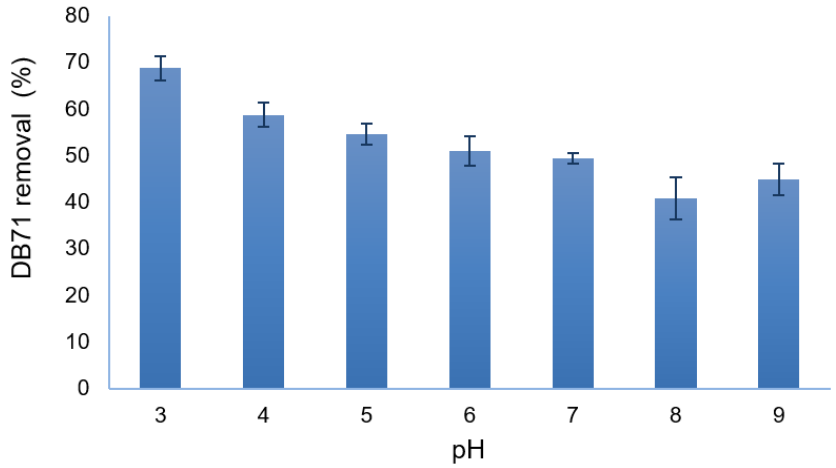


Figure 13. Effect of initial solution pH on DB71 removal by TS ($[DB71]_0$ = 10 mg/L; biosorbent dose = 20 g/L; contact time = 60 min; temperature = 25 °C). Error bars represent the standard deviation from triplicate experiments.

As the pH rises toward neutral and alkaline values, progressive deprotonation of the carboxyl and hydroxyl groups restores and intensifies the negative charge density on the TS surface. Electrostatic repulsion between the increasingly negative surface and the anionic DB71 molecule then opposes the dye approach to the binding sites, and removal efficiency declines. This monotonic decrease with increasing pH is characteristic of anionic-dye adsorption controlled primarily by surface protonation equilibria.

Notably, removal did not collapse under near-neutral conditions: approximately 54% of DB71 was still removed at pH 7, the pH used in the kinetic experiments, compared with the maximum of ~69% at pH 3. While pH adjustment to acidic values maximizes removal—and was therefore adopted for the subsequent isotherm experiments—the substantial capacity retained at pH 7 is practically significant, because real textile effluents are frequently near-neutral, and adsorbents that require strong acidification incur additional chemical and neutralization costs. For this reason, real dyeing effluents

are often treated at their native pH [46]. TS thus offers a favorable balance between removal performance and operational simplicity. The electrokinetic behavior of TS was characterized by zeta potential measurements as a function of pH (Figure S2). The zeta potential is positive below pH 3 and negative above pH 4.2, placing the isoelectric point at approximately pH 4; the crossing occurs between 0.54 mV at pH 3.07 and −0.03 mV at pH 4.20, so the value is given as approximate. This is close to the isoelectric point of pH 3.5 reported for natural guava seeds measured by the same technique [16], and lies at the lower end of the range reported for comparable lignocellulosic and agro-waste materials [47,48]. The measurements reveal two notable features regarding zeta potential. First, the magnitude of the zeta potential is small throughout: it does not exceed 4.4 mV in absolute value at any pH (Figure S2), an order of magnitude below values reported for chitin/lignin [49] (15.5 to −24.5 mV) or for functionalized magnetic sorbents [50] (35 to −20 mV). The TS surface therefore carries a low net charge across the entire pH range examined. Second, the magnitude peaks near pH 7 and returns toward zero at both extremes.

These findings refine the mechanistic understanding of dye removal, indicating that at pH 3, the net surface charge is nearly neutral (0.7 mV), while at pH 7 it is negative (−4.3 mV). Despite a 15% difference in dye removal, the net potential changes by only about 5 mV, suggesting that electrostatic attraction is not the primary driving force. Instead, at acidic pH, protonation of surface groups creates positive binding sites, while at pH 7, non-electrostatic interactions, such as hydrogen bonding, π–π stacking, and hydrophobic interactions, sustain dye uptake. This highlights the complexity of interactions beyond simple charge considerations in dye adsorption processes. This behavior is not unusual for DB71 on lignocellulosic and biopolymeric sorbents. Biglari et al. retained 79.5% of DB71 at pH 11 on pistachio hull waste with a pHpzc of 7.6 [51], and Wawrzkiewicz et al. observed a constant uptake of 9.3 mg/g between pH 2.4 and 8.4 on a chitin/lignin biosorbent with a pHpzc of 8.01 [49]. In both cases, substantial adsorption of the anionic dye persists well above the point of zero charge, indicating that mechanisms other than net electrostatic attraction contribute materially to binding.

The acidic-pH optimum agrees with the general behavior reported for anionic and azo dyes on lignocellulosic biosorbents [52], including the adsorption of DB71 onto wheat shells [19], supporting the broad applicability of this mechanism.

3.8. DB71 biosorption isotherms

Biosorption isotherms describe the equilibrium relationship between the amount of dye adsorbed per unit mass of biosorbent (q_e, mg/g) and the residual dye concentration in solution at equilibrium (C_e, mg/L) at a constant temperature. Isotherms were obtained at three temperatures (25, 35, and 40 °C), and the experimental equilibrium data at the three temperatures are presented together in Figure 14.

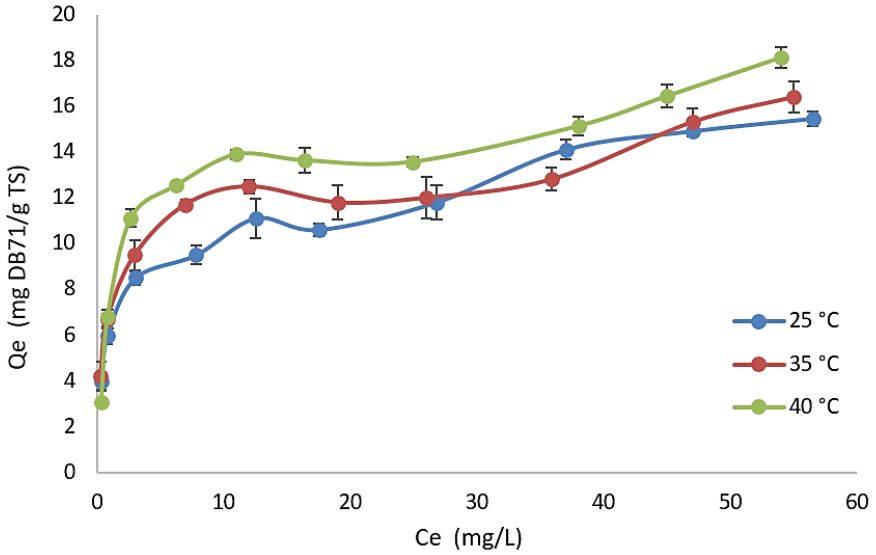


Figure 14. DB71 biosorption isotherms onto tamarind shell (TS) at 25, 35, and 40 °C (biosorbent dose = 20 g/L; pH 3; contact time = 60 min).

The equilibrium isotherms at all three temperatures exhibited a concave-downward profile (Figure 14) that can be classified as an L-type isotherm according to the Giles et al. classification [53]. At low equilibrium concentrations (C_e < 5 mg/L), q_e increased steeply with C_e, reflecting a high initial affinity of DB71 for the TS surface—consistent with the strong electrostatic attraction between the anionic sulfonate groups of DB71 and the protonated, positively charged TS surface at pH 3, as discussed above. As C_e increased, the isotherm slope decreased progressively, indicating gradual occupation of the highest-energy binding sites—primarily the protonated carboxyl and amino groups identified by FTIR—followed by continued but less favorable uptake at lower-affinity sites such as hydroxyl groups and the hydrophobic aromatic domains of the lignin fraction. Notably, q_e continued to increase across the entire concentration range examined, and no saturation plateau was reached under the conditions tested; the capacities reported below should therefore be regarded as operational values for this concentration window rather than as true saturation capacities. Isotherms of this type, in which uptake is governed by binding sites of differing affinity, have been widely reported for the adsorption of anionic dyes onto lignocellulosic materials [54]. Because uptake had not leveled off at the highest concentration examined, the saturation capacity of the system is not determined by these data, and the parameters reported below describe the low- to intermediate-coverage region only.

Furthermore, the equilibrium adsorption capacity q_e increased with temperature across the entire concentration range evaluated (Figure 14), confirming the endothermic nature of the biosorption process: higher temperatures reduce the activation energy barriers for dye diffusion through the external boundary layer and into internal pore sites, increasing the accessibility of lower-affinity binding sites and thus enhancing overall uptake [55]. This temperature dependence is further discussed in the context of the thermodynamic parameters presented below.

In addition, the experimental data were fitted to three widely used isotherm models: the Langmuir, Freundlich, and Langmuir–Freundlich (Sips) models, whose equations and parameters are well known [56]. Fitting was performed using nonlinear regression in Statistica v7.0, and Table 2 presents

the isotherm model parameters for DB71 biosorption obtained with each model at the tested temperatures.

Table 2. Isotherm model parameters and model-selection statistics for DB71 biosorption onto tamarind shell (TS) at 25, 35, and 40 °C (biosorbent dose = 20 g/L; pH 3; contact time = 60 min).

T (°C)	Model	Parameters	R	R^2	R^2_{adj}	RMSE	AIC_c	ΔAIC_c
25	Langmuir	Q_0 = 13.66 mg/g; b = 0.6543 L/mg	0.900	0.810	0.762	1.529	18.50	19.30
25	Freundlich	K_F = 5.945; n = 4.27	0.985	0.970	0.965	0.583	−0.80	0
25	Langmuir–Freundlich	K_{LF} = 7.326; a_{LF} = 0.0103; n_{LF} = 0.325	0.985	0.970	0.961	0.574	4.89	5.69
35	Langmuir	Q_0 = 13.84 mg/g; b = 1.0104 L/mg	0.925	0.856	0.816	1.317	15.51	4.86
35	Freundlich	K_F = 6.988; n = 5.09	0.958	0.918	0.887	1.033	10.65	0
35	Langmuir–Freundlich	K_{LF} = 10.024; a_{LF} = 0.4656; n_{LF} = 0.389	0.963	0.927	0.882	0.980	15.59	4.94
40	Langmuir	Q_0 = 15.73 mg/g; b = 0.8104 L/mg	0.964	0.929	0.911	1.118	12.23	0
40	Freundlich	K_F = 7.219; n = 4.72	0.948	0.899	0.866	1.374	16.36	4.13
40	Langmuir–Freundlich	K_{LF} = 11.350; a_{LF} = 0.6551; n_{LF} = 0.663	0.972	0.945	0.915	1.014	16.27	4.04

R, correlation coefficient; R^2_{adj}, adjusted coefficient of determination; RMSE, root-mean-square error (mg/g); AIC_c, Akaike information criterion corrected for small sample size. ΔAIC_c refers to the best-supported model at each temperature.

As the correlation coefficient on its own cannot discriminate between models of different complexity, the three models were compared based on the adjusted R^2, the root-mean-square error, and the small-sample corrected Akaike information criterion (AICc) [57], which penalizes the additional parameter of the Sips equation (Table 2). The Freundlich model is best supported at 25 and 35 °C, and the Langmuir model at 40 °C; the Langmuir–Freundlich model is not selected at any temperature, with ΔAICc relative to the best-supported model of 5.69, 4.94, and 4.04, respectively. The adjusted R^2 at 40 °C shows a very slight preference for the Sips equation (0.915 vs. 0.911), so the two criteria are not unanimous at this temperature, and both are reported. The reason for the identical correlation coefficients (R = 0.985) obtained at 25 °C by the Freundlich and Sips equations is that the determinant of the Sips equation varies only between 1.010 and 1.039 over the measured range with the fitted parameters, so the saturation term is inactive, and the equation degenerates to a Freundlich power law. Refitting the Sips model at 25 °C with neutral starting values converges on a negative a_{LF}, which confirms that this parameter is not identifiable from the present data. The Langmuir model was the

worst fit at 25 and 35 °C but was better than the Freundlich model at 40 °C (R = 0.964 vs. 0.948).

The best fit to the Freundlich model at the two lower temperatures suggests adsorption onto a surface with binding sites of different affinities across the coverage range investigated. This is physically consistent with the rough, heterogeneous morphology of TS observed by SEM and with the multiple functional groups identified by FTIR. The Freundlich exponents n are >1 (4.27, 5.09, and 4.72 at 25, 35, and 40 °C), corresponding to an L-type (concave-downward) isotherm in which sorption becomes less favorable as higher-energy sites fill; the temperature variation is nonmonotonic and is not further interpreted. The Langmuir Q_o values (13.66, 13.84, and 15.73 mg/g) increase with temperature, in the expected direction for an endothermic process, but are not saturation capacities: no plateau was reached, and the maximum experimental uptake exceeds Q_o at every temperature by 13.1%, 18.5%, and 15.1% at 25, 35, and 40 °C, respectively. The saturation capacity implied by the Sips parameters is still less well determined, taking values of 71.1, 21.5, and 17.3 mg/g across a 15 °C interval. This variation reflects the absence of a plateau rather than any property of the material. Finally, the residuals of the best-supported model show the same sign pattern at all three temperatures, negative between $C_e \approx 17$ and 38 mg/L and positive at both ends of the range, indicating a systematic feature of the isotherm that none of the three models reproduces. Denser equilibrium data over a longer concentration range would be necessary to characterize it and to constrain the saturation capacity.

Table 3 compares the Langmuir maximum adsorption capacity (Q_0) of TS with those reported for other adsorbents evaluated for DB71 removal. The Q_0 obtained in this study (13.66 mg/g at 25 °C, pH 3) reflects the moderate but functional adsorption capacity of natural, unmodified tamarind shell. As shown in Table 3, this value coincides with that reported for surfactant-modified zeolite (clinoptilolite, 13.66 mg/g) and exceeds only a subset of the materials listed; it is surpassed by chemically modified and thermally processed adsorbents, including chitosan-MWCNT nanocomposites, chitin/lignin biosorbents, and magnetic ionic liquid-functionalized materials, as well as by other unmodified natural biosorbents such as wheat shells, pistachio hull waste, and organic-rich compost. However, direct comparison of Langmuir Q_0 values across studies is inherently limited by differences in experimental conditions—particularly initial dye concentration range, temperature, pH, and biosorbent dose—which strongly influence the fitted parameters. In this study, isotherms were constructed at 10 initial concentrations spanning 60–420 mg/L at pH 3, with a biosorbent dose of 20 g/L. In contrast, several studies in the literature used different pH values and narrower concentration ranges, which may favor higher apparent Q_0 values. Importantly, the moderate Langmuir Q_0 of unmodified TS does not fully capture its performance, because no saturation plateau was reached, and Q_0 is therefore an operational fitting constant rather than a monolayer capacity: the maximum experimental uptake exceeded it by 13.1%, 18.5%, and 15.1% at 25, 35, and 40 °C, respectively (15.45, 16.40, and 18.11 mg/g). Furthermore, the TS+Pc combined system achieves removal efficiencies that far surpass what the biosorbent capacity alone would suggest by coupling biosorption with enzymatic biodegradation. These results position unmodified TS as a functionally competitive, zero-cost biosorbent whose practical performance in combined systems extends well beyond what isotherm parameters alone convey.

Table 3. Fitted Langmuir constants (Q_0) reported for Direct Blue 71 removal by tamarind shell (TS) and other adsorbents, together with the experimental conditions under which each was obtained.

Adsorbent	Modification	Q_o (mg/g)*	C_0 range (mg/L)	Adsorbent dose	T (°C)	Optimal pH	Reference
Tamarind shell	None	13.66	60–420	20 g/L	25	3	This study
Wheat shells	None	46.3	50–250	10 g/L	40	7	[19]
Pistachio hull waste	None	90.48	10–100	0.1 g/L	50	2	[51]
Organic-rich compost	None	95.4	400	0.40 g	50	3.0	[58]
Chitin/lignin biosorbent	None (biopolymer blend)	40	50–1000	10 g/L	ambient	2.4–8.4	[49]
Modified zeolite (clinoptilolite)	Surfactant-modified	13.66	25–100	2.5–12.5 g	23 ± 1	3	[59]
$NiFe_2O_4$/clinoptilolite nanoparticles	$NiFe_2O_4$ nanoparticle	6.31	60	0.6 g/L	25	6	[60]
Chitosan-MWCNT nanocomposite	Multi-walled carbon nanotubes	29.32	10–80	1 g/L	n.r.	6	[61]
Magnetic ionic liquid (γ-Fe_2O_3-2-HEAS)	Ionic liquid	47.60	10–60	1.09 g/L	n.r.	3.5	[50]

*Values were determined under heterogeneous conditions and are not directly comparable.

The thermodynamic parameters for DB71 biosorption onto TS were derived from the equilibrium constants obtained at the three temperatures studied. To avoid the inconsistencies that arise when a dimensioned equilibrium constant is introduced into the Van't Hoff equation, the Langmuir constant b (L/mg) was converted into a dimensionless thermodynamic equilibrium constant (K°) following the procedure recommended by Tran et al. [39]: $K^\circ = (b \times M_{DB71} \times 10^3)/C^\circ$, in which the factor 10^3 converts b from L/mg to L/g, the molar mass M_{DB71} = 1029.87 g/mol converts it further to L/mol, and division by the standard concentration C° = 1 mol/L renders the constant dimensionless; the activity coefficient was taken as unity, as recommended for the dilute solutions employed here. The resulting K° values were 6.74×10^5, 1.04×10^6, and 8.35×10^5 at 25, 35, and 40 °C, respectively. The standard Gibbs free energy was calculated as $\Delta G^\circ = -RT \ln K^\circ$, and ΔH° and ΔS° were obtained from the slope and intercept of the Van't Hoff plot of $\ln K^\circ$ vs. $1/T$. The corresponding values are summarized in Table S1.

The ΔG° values were negative at all three temperatures (−33.27, −35.50, and −35.50 kJ/mol at 25, 35, and 40 °C, respectively), indicating that the biosorption of DB71 onto TS is thermodynamically spontaneous under the conditions tested, in agreement with the substantial removal efficiencies observed experimentally. These ΔG° values are robust to the uncertainty in the underlying isotherm fit:

because ΔG° depends on the logarithm of K°, an error of a factor of two in *b* would displace ΔG° by only 1.7 kJ/mol, so the conclusion of spontaneity does not depend on the precision of the Langmuir constant. The enthalpic and entropic terms, in contrast, are not determined by the present data. The Van't Hoff regression over three temperatures returns $R^2 = 0.43$, and refitting to each temperature pair in turn gives ΔH° = 33.2, 11.1, and −35.4 kJ/mol for the 25/35, 25/40, and 35/40 °C pairs; the sign of the enthalpy change is therefore unresolved. The values of ΔH° and ΔS° listed in Table S1 are reported for completeness only and should not be interpreted quantitatively; no mechanistic inference is drawn from the magnitude of ΔH° here. The process is endothermic, as established independently by the increase in uptake with temperature described previously, and the physisorption-dominated character of the interaction rests on the spectroscopic and pH-dependence evidence rather than the fitted enthalpy. Reliably determining ΔH° and ΔS° would require equilibrium data at five or more temperatures.

3.9. Fixed-bed column dye removal experiments

Fixed-bed column systems offer significant practical advantages over batch systems for the continuous treatment of dye-contaminated effluents, as the adsorbent is maintained in constant contact with fresh influent, maximizing the concentration gradient and thus the driving force for adsorption throughout the operation [62]. In this study, fixed-bed column experiments were performed using two packing configurations: tamarind shell alone (TS) and tamarind shell inoculated with *Phanerochaete chrysosporium* (Pc), hereafter referred to as TS+Pc. Figure S3 shows the experimental arrangement. Both columns were operated under identical conditions, as mentioned above. Breakthrough was defined as the point at which the effluent concentration reached 50% of the influent concentration ($C/C_0 = 0.5$). Figures 15 and 16 show the breakthrough curves for both systems and the fitted column model curves for the TS and TS+Pc columns, respectively, plotting C/C_0 vs. time. Table 4 summarizes the estimated model parameters.

3.9.1. DB71 removal in the TS column

The breakthrough curve for the TS column exhibited a characteristic sigmoidal profile, with effluent concentration increasing progressively over time, reflecting gradual bed saturation from the inlet downward as active binding sites became occupied (Figure 15). Breakthrough ($C/C_0 = 0.5$) was reached at an experimental breakthrough time of τexp = 25 min, and the column reached its maximum effluent concentration at approximately 60 min of operation. This relatively short breakthrough time reflects the inherent limitation of unmodified natural biosorbents operating under continuous-flow conditions, where contact time between the adsorbate and the bed is significantly shorter than in batch systems.

To describe the dynamic behavior of the TS column, three empirical models were fitted to the breakthrough curve data: the Yoon–Nelson, dose-response, and Thomas models. As summarized in Table 4, both the Yoon–Nelson and Thomas models provided excellent fits to the experimental data, with identical $R^2 = 0.9980$, while the dose-response model achieved the highest correlation ($R^2 = 0.9988$). However, although the dose-response model yields the highest R^2, its parameters are empirical curve-shape descriptors rather than physically grounded transport or kinetic constants, which limits its interpretability and usefulness for scaling up column operations [63]. Among the near-equivalent fits,

the Yoon–Nelson model is therefore adopted as the primary descriptor for this column, not on the grounds of statistical superiority—the R^2 differences among the three models are below 10^{-3}—but because its parameters τ and q_0 carry direct operational meaning for column design. It should be noted that the Thomas and Yoon–Nelson equations are algebraic reparameterizations of the same logistic expression, related by $K_{YN} = K_{Th} \cdot C_0$ and $\tau = q_0 \cdot m/(C_0 \cdot Q)$; their identical R^2 and q_0 values in Table 4 are therefore an expected mathematical consequence and do not constitute independent corroboration.

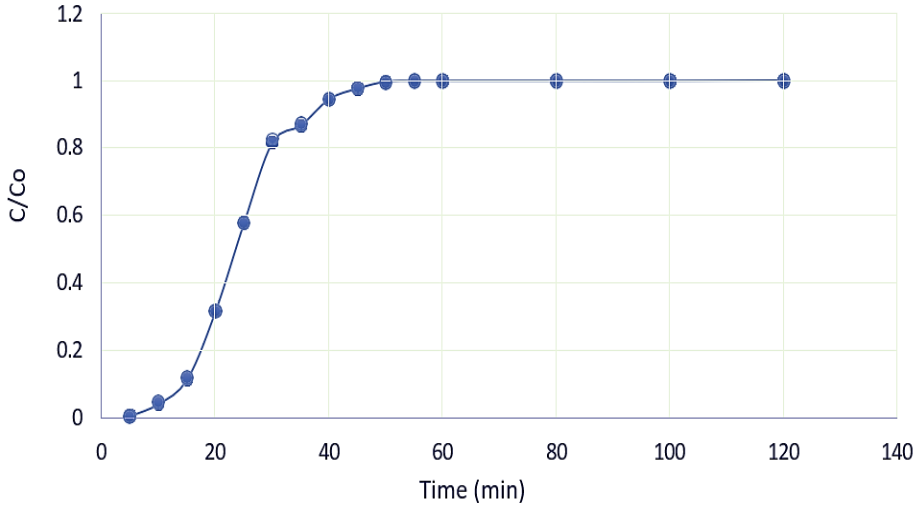


Figure 15. Breakthrough curve for DB71 removal in the fixed-bed column packed with TS alone ($[DB71]_0$ = 10 mg/L; bed height = 15 cm; flow rate = 1 mL/min; temperature = 35 °C).

The Yoon–Nelson model yielded a calculated breakthrough time of τ_{calc} = 23.73 min, in close agreement with the experimentally observed value of τ_{exp} = 25 min, confirming the model's ability to accurately capture the breakthrough dynamics. The rate constant KYN = 0.2179 min^{-1} reflects the relatively steep slope of the TS breakthrough curve (Figure 15), consistent with fast mass-transfer kinetics and rapid bed saturation. The corresponding bed capacity at breakthrough, estimated using the Yoon–Nelson model, was q_0 = 2.51 μg/g, based on the 94.6 g of TS packed in the bed. This value is two orders of magnitude below the equilibrium uptake measured in batch experiments at the same initial concentration ($q_e \approx 0.52$ mg/g at C_0 = 10 mg/L, biosorbent dose = 10 g/L), which is the expected consequence of the very different solid-to-liquid ratios of the two configurations: only 25 mL of solution had passed through the bed at breakthrough, giving an effective ratio of approximately 3800 g/L against 10 g/L in the batch experiments. At breakthrough, the bed had therefore expressed less than 0.5% of its equilibrium capacity, indicating that breakthrough in this configuration was governed by the residence time available for mass transfer rather than by exhaustion of binding sites. Column capacity per unit mass and batch equilibrium capacity are therefore not directly comparable, and the low value of q_0 reflects poor bed utilization under the operating conditions used rather than a deficiency of the biosorbent.

The flow regime provides a further constraint on this interpretation. The columns were dry-packed and fed by gravity at 1 mL/min, a superficial velocity of 0.08 cm/min, under which the bed operates in an unsaturated trickle-flow regime rather than as a flooded packed bed. The volume of liquid in

contact with the solid at any instant is therefore a small fraction of the geometric void volume of 188.5 cm^3, which accounts for the limited fraction of the equilibrium capacity expressed at breakthrough. Liquid holdup was not measured, and the fitted parameters should accordingly be regarded as operational descriptors of this configuration rather than as transport constants. Since both columns were packed by the same procedure and operated under identical conditions, the comparison between configurations is unaffected.

3.9.2. DB71 removal in the TS+Pc column

The breakthrough curve for the TS+Pc column showed a markedly different profile than the TS column (Figure 16), with a slow initial rise followed by a more rapid increase toward saturation—a two-phase shape reflecting simultaneous biosorption and enzymatic degradation. Breakthrough ($C/C_0 = 0.5$) was reached at $\tau exp = 82$ min, and the effluent concentration had risen to $C/C_0 \approx 0.96$ by 160 min, at which point the run was terminated; unlike the TS column, the TS+Pc bed had therefore not reached full exhaustion within the operating window—representing an increase of approximately 3.3-fold in breakthrough time relative to the TS column alone. This substantial extension of the operational lifetime of the column is attributed to the combined action of two simultaneous removal mechanisms in the TS+Pc system: biosorption of DB71 onto the TS surface and onto the fungal biomass, and enzymatic degradation of the dye by the ligninolytic enzyme system of *Pc*, which produces manganese peroxidase (MnP) and lignin peroxidase (LiP) capable of oxidatively cleaving the azo bonds of DB71 [13]. The coexistence of these two mechanisms—biosorption and biodegradation—results in a synergistic enhancement of DB71 removal that extends bed exhaustion well beyond what either TS or *Pc* could achieve individually.

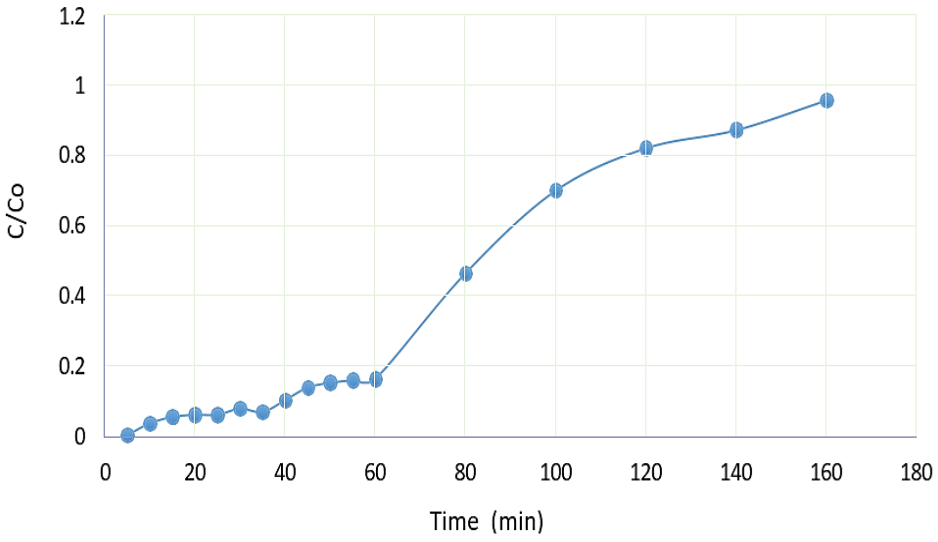


Figure 16. Breakthrough curve for DB71 removal in the fixed-bed column packed with tamarind shell inoculated with *Phanerochaete chrysosporium* (TS+Pc) ($[DB71]_0 = 10$ mg/L; bed height = 15 cm; flow rate = 1 mL/min; temperature = 35 °C).

As in the TS column, the Yoon–Nelson model provided the best balance of goodness of fit and physical interpretability for the TS+Pc breakthrough curve (R^2 = 0.9928), followed by the dose-response model (R^2 = 0.9903). The Thomas model yielded an identical R^2 to the Yoon–Nelson model (0.9928) but should be interpreted with caution: the asymmetric, two-phase shape of the TS+Pc breakthrough curve fundamentally violates the Thomas model's assumption of a symmetric sigmoidal profile, meaning that while the numerical fit is acceptable, the model does not correctly represent the underlying physical process [64]. The Yoon–Nelson model yielded a calculated breakthrough time of τ_{calc} = 86.38 min, in reasonable agreement with the experimentally observed value of τ_{exp} = 82 min. The rate constant K_{YN} = 0.0473 min^{-1} is substantially lower than that of the TS column (0.2179 min^{-1}), quantitatively reflecting the more gradual breakthrough progression sustained by the additional enzymatic removal mechanism. The estimated bed capacity at breakthrough was q_0 = 8.39 μg/g, referred to the 103 g of TS+Pc packed in the bed, representing a 3.3-fold increase relative to the TS column alone (q_0 = 2.51 μg/g) and further quantifying the potentiating effect of *Pc* inoculation on the column's overall removal performance. The dose-response model yielded q_0 = 8.00 μg/g, consistent with the Yoon–Nelson estimate. Integration of the breakthrough curves over the full duration of each run gives a total retained dye mass 3.6 times greater for TS+Pc than for TS, confirming the magnitude of the enhancement by a route independent of any model.

3.9.3. Comparative analysis of the TS and TS+Pc column systems

A direct comparison of the two column systems reveals that inoculating TS with *Pc* consistently improved all key performance indicators of the fixed-bed system (Table 4). The experimental breakthrough time increased from 25 to 82 min; the TS column was fully exhausted after approximately 60 min, whereas the TS+Pc column had still not reached saturation when the run was terminated at 160 min; and the bed capacity at breakthrough (Yoon–Nelson) increased from 2.51 to 8.39 μg/g—a 3.3-fold improvement, referred to packed masses of 94.6 and 103 g, respectively. These comparisons depend on the breakthrough criterion adopted. Applying the more conservative definition of C/C_0 = 0.1 gives breakthrough times of 14.3 and 39.4 min and bed capacities of 1.47 and 3.63 μg/g for TS and TS+*Pc*, respectively, corresponding to enhancement factors of 2.8 and 2.5. The advantage conferred by fungal inoculation is thus attenuated but not eliminated under the stricter criterion, lying between two- and three-fold on either definition. These results are consistent with the batch decolorization experiments described above, where the TS+Pc system achieved substantially higher DB71 removal efficiencies than either component alone across all initial dye concentrations tested, and confirm that the synergistic biosorption–biodegradation mechanism observed in batch mode translates effectively to a continuous-flow column configuration. The ability of *Pc* to use TS as a lignocellulosic carbon source—evidenced by its rapid colonization of the biosorbent surface within 6–7 days of inoculation—likely sustains fungal metabolic activity and ligninolytic enzyme production during column operation, maintaining the system's degradative capacity over extended periods and preventing the rapid exhaustion observed in the TS-alone column.

In both column systems, the Yoon–Nelson model provided the most operationally useful parameterization of the breakthrough behavior, although its symmetric logistic form is a recognized limitation for the asymmetric TS+Pc front; for that system, the experimentally determined breakthrough time is the more reliable design quantity. Developing a column model that explicitly

couples biosorption with enzymatic degradation remains an open objective. As discussed in Section 3.9.1, the bed capacities at breakthrough (q_0 = 2.51 and 8.39 μg/g for TS and TS+Pc, respectively) lie far below the batch equilibrium uptake ($qe \approx 0.52$ mg/g), because the volume of solution treated up to breakthrough is small relative to the mass of packed biosorbent; both beds were therefore operating well short of saturation. Future optimization of column geometry—particularly by reducing the flow rate or increasing bed height—could further extend breakthrough times and improve overall removal efficiency for practical textile wastewater treatment applications.

Table 4. Column model parameters and correlation coefficients (R^2) for DB71 removal in fixed-bed columns packed with TS and TS+Pc, fitted to the Yoon–Nelson, dose-response, and Thomas models.

Model/parameter	Biosorbent	
	TS	TS+Pc
Yoon–Nelson		
K_{YN} (min^{-1})	0.2179	0.0473
τ calc (min)	23.73	86.38
τ exp (min)	25.00	82.00
q_o (μg/g)	2.51	8.39
R^2	0.9980	0.9928
Dose-response		
A (dimensionless)	5.12	3.74
B (min)	23.2	82.43
q_o (μg/g)	2.44	8.0
R^2	0.9988	0.9903
Thomas		
K_{Th} (L/min.mg)	0.0216	0.0047
Q (mL/min)	1	1
q_o (μg/g)	2.51	8.39
R^2	0.9980	0.9928

4. Conclusions

This study demonstrated that tamarind shell (*Tamarindus indica*, TS) is an effective, low-cost, unmodified lignocellulosic biosorbent for the removal of Direct Blue 71 (DB71) from aqueous solutions, and that its performance is substantially enhanced when used as an immobilization support for *Phanerochaete chrysosporium* (Pc). Collectively, the results support the hypothesis that a single agricultural by-product can fulfill a dual active role—as a primary biosorbent for rapid dye capture and as a nutrient-rich lignocellulosic substrate that sustains and stimulates fungal degradative activity—yielding a system whose combined performance substantially exceeds that of either component operated alone.

Physicochemical characterization of TS revealed a heterogeneous, porous surface rich in hydroxyl, carboxyl, carbonyl, and amino functional groups available to bind the anionic DB71 molecule.

Biosorption kinetics were adequately described by the pseudo-second-order, pseudo-first-order, and Elovich equations, which were statistically near-equivalent for the present data set; the mechanistic interpretation therefore rests on spectroscopic, pH-dependent, and thermodynamic evidence, which together indicate an interaction driven by electrostatic attraction and hydrogen bonding. Model selection based on the corrected Akaike information criterion supported the Freundlich isotherm at 25 and 35 °C and the Langmuir isotherm at 40 °C, indicating adsorption onto a surface with binding sites of differing affinity over the coverage range examined; the system's saturation capacity was not determined because it did not reach a plateau. While the Langmuir Q_0 of unmodified TS is moderate relative to chemically modified adsorbents, the practical removal performance of TS—particularly in the combined TS+Pc system—extends well beyond what this single parameter conveys, underscoring the value of integrating biosorption with enzymatic biodegradation. The increase in adsorption capacity with temperature further suggests that elevated operating temperatures, as encountered in textile effluents, are advantageous for practical applications.

The successful colonization of TS by *Pc* within 6–7 days and the fungus's demonstrated capacity to enzymatically degrade DB71 even under nutrient-limited conditions established the biological foundation of the combined system. Critically, the lignocellulosic nature of TS proved essential not merely as a physical support but as a metabolic inducer that sustained fungal growth and ligninolytic enzyme production—particularly at dye concentrations that otherwise inhibited fungal activity. This dual functionality translated directly into enhanced performance in both batch and continuous-flow configurations: in the fixed-bed column, the TS+Pc system achieved a 3.3-fold increase in breakthrough time (from 25 to 82 min) and a 3.3-fold increase in bed capacity at breakthrough (from 2.51 to 8.39 μg/g) relative to TS alone, confirming that the synergistic biosorption–biodegradation mechanism is operationally robust under continuous-flow conditions.

The study's limitation is the absence of a TS-only treatment and a non-viable fungal biomass control in liquid-phase experiments. While the combined system shows superior performance, it does not allow for quantifying the contributions of biosorption and enzymatic degradation. To address this, the study needs these controls, along with identification of degradation products and assessment of ligninolytic enzyme activity, to determine whether decolorization leads to mineralization or the accumulation of potentially toxic colorless aromatic amines.

Overall, this work establishes tamarind shell-immobilized *P. chrysosporium* as a promising, sustainable, and scalable platform for the treatment of azo dye-contaminated textile wastewater, combining the economic advantages of agricultural waste valorization with the degradative power of white-rot fungal biotechnology. Future work should focus on optimizing column geometry and operating conditions, evaluating regeneration and reuse cycles, assessing performance with real textile effluents, and quantifying the enzymatic activity responsible for dye degradation to further elucidate the relative contributions of biosorption and biodegradation to overall removal.

Use of AI tools declaration

The authors declare they have not used Artificial Intelligence (AI) tools in the creation of this article.

Acknowledgments

We thank SECIHTI for the scholarship awarded to A.D. Mota-Gutiérrez, and we thank S. Valencia-Leal for technical support. We also thank SECIHTI for the financial support provided under project number PEE-2025-G-209.

Conflict of interest

The authors declare no conflicts of interest.

References

1. Berradi M, Hsissou R, Khudhair M, et al. (2019) Textile finishing dyes and their impact on aquatic environs. Heliyon 5.
2. Yaseen DA, Scholz M (2019) Textile dye wastewater characteristics and constituents of synthetic effluents: a critical review. *Int J Environ Sci Technol* 16: 1193–1226. https://doi.org/10.1007/s13762-018-2130-z
3. Roy A, Adhikari B, Majumder SB (2013) Equilibrium, Kinetic, and Thermodynamic Studies of Azo Dye Adsorption from Aqueous Solution by Chemically Modified Lignocellulosic Jute Fiber. *Ind Eng Chem Res* 52: 6502–6512. https://doi.org/10.1021/ie400236s
4. Ertugay N, Acar FN (2017) Removal of COD and color from Direct Blue 71 azo dye wastewater by Fenton's oxidation: Kinetic study. *Arab J Chem* 10: S1158–S1163. https://doi.org/10.1016/j.arabjc.2013.02.009
5. Maleki S, Ghorbani S, Monajemi P (2023) Decolorization of azo Direct Blue 71 dye in aqueous solutions using sequential upflow anaerobic sludge blanket reactor and UV/H2O2 process. *Biochem Eng J* 199: 109057. https://doi.org/10.1016/j.bej.2023.109057
6. Hamad HN, Idrus S (2022) Recent Developments in the Application of Bio-Waste-Derived Adsorbents for the Removal of Methylene Blue from Wastewater: A Review. *Polymers* 14. https://doi.org/10.3390/polym14040783
7. Ali K, Zeidan H, Amar RB (2023) Evaluation of the use of agricultural waste materials as low-cost and eco-friendly sorbents to remove dyes from water: a review. *Desalin Water Treat* 302: 231–252. https://doi.org/10.5004/dwt.2023.29725
8. Buhani, Putri HY, Nasution MhdAA, et al. (2025) Magnetite-coated and silanized carbon from rubber fruit shells for synthetic dye removal. *Microchem J* 219: 116125. https://doi.org/10.1016/j.microc.2025.116125
9. Lawrence NA, Siddiqui S, Isaac R, et al. (2026) Waste-to-resource approach: Sustainable synthesis and life cycle assessment of rice husk char-supported Mg–Al layered double hydroxide for dye biosorption. *Sustain Chem Pharm* 52: 102474. https://doi.org/10.1016/j.scp.2026.102474
10. Garcia-Amezquita LE, Tejada-Ortigoza V, Heredia-Olea E, et al. (2018) Differences in the dietary fiber content of fruits and their by-products quantified by conventional and integrated AOAC official methodologies. *J Food Compos Anal* 67: 77–85. https://doi.org/10.1016/j.jfca.2018.01.004

11. Amulani A, Nandanwar T, Baskaran K, et al. (2023) Characterization of tamarind biomass to substantiate the feasibility towards alternative fuel. *Sustaina Energy Technol Assess* 56: 103056. https://doi.org/10.1016/j.seta.2023.103056
12. Costa FCR, Brito FSL, Grandi MJR de, et al. (2025) White Rot Fungi for Biodegradation of Dyes: Potential for Industrial Uses - A Review. *J Braz Chem Soc* 36: e.
13. Liu S, Xu X, Kang Y, et al. (2020) Degradation and detoxification of azo dyes with recombinant ligninolytic enzymes from Aspergillus sp. with secretory overexpression in Pichia pastoris. *R Soc Open Sci* 7: 200688. https://doi.org/10.1098/rsos.200688
14. Santos ADO, Bandeira L, Silva GMM, et al. (2021) Use of Phanerochaete Chrysosporium in a Semibatch Reactor for Removal of Indigo Carmine from Synthetic Textile Wastewater. *Braz arch biol technol* 64: e21200503. https://doi.org/10.1590/1678-4324-2021200503
15. Bié J, Sepodes B, Fernandes PCB, et al. (2022) Enzyme Immobilization and Co-Immobilization: Main Framework, Advances and Some Applications. *Processes* 10. https://doi.org/10.3390/pr10030494
16. Tapia-Quiroz GE, Valencia-Leal SA, Vázquez-Guerrero A, et al. (2025) Surfactant-Enhanced Guava Seed Biosorbent for Lead and Cadmium Removal: Kinetics, Thermodynamics, and Reusability Insights. *Sustain Chem* 6: 5. https://doi.org/10.3390/suschem6010005
17. Soury R, Teka S, Alenezi KM, et al. (2023) Characterization and application of ligno-cellulosic fibers derived from Robinia Pseudoacacia for the bio-sorption of methylene blue from water. *Int J Phytoremediat* 25: 1359–1370. https://doi.org/10.1080/15226514.2022.2158782
18. Mihai S, Bondarev A, Călin C, et al. (2024) Adsorbent Biomaterials Based on Natural Clays and Orange Peel Waste for the Removal of Anionic Dyes from Water. *Processes* 12. https://doi.org/10.3390/pr12051032
19. Bulut Y, Gözübenli N, Aydın H (2007) Equilibrium and kinetics studies for adsorption of direct blue 71 from aqueous solution by wheat shells. *J Hazard Mater* 144: 300–306. https://doi.org/10.1016/j.jhazmat.2006.10.027
20. Chan K-T, Ong S-T, Ha S-T (2024) Adsorptive removal of Congo Red dye from its aqueous solutions by tetraethylenepentamine modified peanut husks composite beads. *Desalin Water Treat* 317: 100060. https://doi.org/10.1016/j.dwt.2024.100060
21. Broche Galindo MH, Rodríguez Rico IL, Coca Rives Y, et al. (2018) Caracterización de los residuos agrícolas de sorgo para su uso como material biosorbente de colorantes. *Centro Azúcar* 45: 64–75.
22. Gaur B, Mittal J, Shah SAA, et al. (2024) Sequestration of an Azo Dye by a Potential Biosorbent: Characterization of Biosorbent, Adsorption Isotherm and Adsorption Kinetic Studies. *Molecules* 29. https://doi.org/10.3390/molecules29102387
23. Stark NM, Matuana LM (2007) Characterization of weathered wood–plastic composite surfaces using FTIR spectroscopy, contact angle, and XPS. *Polym Degrad Stabil* 92: 1883–1890. https://doi.org/10.1016/j.polymdegradstab.2007.06.017
24. Poletto M, Zattera AJ, Santana RMC (2012) Structural differences between wood species: Evidence from chemical composition, FTIR spectroscopy, and thermogravimetric analysis. *J Appl Polym Sci* 126: E337–E344. https://doi.org/10.1002/app.36991

25. Sun RC, Tomkinson J (2002) Characterization of hemicelluloses obtained by classical and ultrasonically assisted extractions from wheat straw. *Carbohydr Polym* 50: 263–271. https://doi.org/10.1016/S0144-8617(02)00037-1
26. Sivaraj R, Namasivayam C, Kadirvelu K (2001) Orange peel as an adsorbent in the removal of Acid violet 17 (acid dye) from aqueous solutions. *Waste Manage* 21: 105–110. https://doi.org/10.1016/S0956-053X(00)00076-3
27. Kasbaji M, Mennani M, Grimi N, et al. (2023) Adsorption of cationic and anionic dyes onto coffee grounds cellulose/sodium alginate double-network hydrogel beads: Isotherm analysis and recyclability performance. *Int J Biol Macromol 2*39: 124288. https://doi.org/10.1016/j.ijbiomac.2023.124288
28. Li Y, Du Q, Liu T, et al. (2013) Comparative study of methylene blue dye adsorption onto activated carbon, graphene oxide, and carbon nanotubes. *Chemical Engineering Research and Design* 91: 361–368. https://doi.org/10.1016/j.cherd.2012.07.007
29. Verma P, Madamwar D (2002) Production of ligninolytic enzymes for dye decolorization by cocultivation of white-rot fungi Pleurotus ostreatus and Phanerochaete chrysosporium under solid-state fermentation. *Appl Biochem Biotechnol* 102: 109–118. https://doi.org/10.1385/ABAB:102-103:1-6:109
30. Villa Y, Espín N (2012) Determinación de la cinética de crecimiento del hongo Phanerochaete chrysosporium en residuos lignocelulósicos y determinación de la actividad ligninoperoxidásica. *Revista Politécnica* 31.
31. Zhi Z, Wang H (2014) White-rot fungal pretreatment of wheat straw with Phanerochaete chrysosporium for biohydrogen production: simultaneous saccharification and fermentation. *Bioprocess Biosyst Eng* 37: 1447–1458. https://doi.org/10.1007/s00449-013-1117-x
32. Mehmood A, Hussain A, Irshad M, et al. (2019) Cinnamic acid as an inhibitor of growth, flavonoids exudation and endophytic fungus colonization in maize root. *Plant Physiol Biochem* 135: 61–68. https://doi.org/10.1016/j.plaphy.2018.11.029
33. Moreira MT, Feijoo G, Palma C, et al. (1997) Continuous production of manganese peroxidase by Phanerochaete chrysosporium immobilized on polyurethane foam in a pulsed packed-bed bioreactor. *Biotechnol Bioeng* 56: 130–137. https://doi.org/10.1002/(SICI)1097-0290(19971020)56:2<130::AID-BIT2>3.0.CO;2-Q
34. Nilsson I, Möller A, Mattiasson B, et al. (2006) Decolorization of synthetic and real textile wastewater by the use of white-rot fungi. *Enzyme Microb Technol* 38: 94–100. https://doi.org/10.1016/j.enzmictec.2005.04.020
35. Aksu Z (2005) Application of biosorption for the removal of organic pollutants: a review. *Process Biochem* 40: 997–1026. https://doi.org/10.1016/j.procbio.2004.04.008
36. Ho YS, McKay G, Wase DAJ, et al. (2000) Study of the Sorption of Divalent Metal Ions on to Peat. *Adsorpt Sci Technol* 18: 639–650. https://doi.org/10.1260/0263617001493693
37. Low M.J.D. (1960). Kinetics of chemisorption of gases on solids. *Chem Rev* 60: 267–312. https://doi.org/10.1021/cr60205a003
38. Lagergren S. (1898). Zur Theorie der sogenannten Adsorption gelöster Stoffe. Kungliga Svenska Vetenskapsakademiens Handlingar 24: 1–39

39. Tran HN, You S-J, Hosseini-Bandegharaei A, et al. (2017) Mistakes and inconsistencies regarding adsorption of contaminants from aqueous solutions: A critical review. *Water Res* 120: 88–116. https://doi.org/10.1016/j.watres.2017.04.014
40. Simonin J-P (2016) On the comparison of pseudo-first order and pseudo-second order rate laws in the modeling of adsorption kinetics. *Chem Eng J* 300: 254–263. https://doi.org/10.1016/j.cej.2016.04.079
41. Wu F-C, Tseng R-L, Juang R-S (2009) Characteristics of Elovich equation used for the analysis of adsorption kinetics in dye-chitosan systems. *Chem Eng J* 150: 366–373. https://doi.org/10.1016/j.cej.2009.01.014
42. Tang Y, Chen L, Wei X, et al. (2013) Removal of lead ions from aqueous solution by the dried aquatic plant, Lemna perpusilla Torr. *J Hazard Mater* 244–245: 603–612. https://doi.org/10.1016/j.jhazmat.2012.10.047
43. Overah LC (2020) Nonlinear Kinetic and Equilibrium Adsorption Isotherm Study of Cadmium (II) Sorption by Dacryodes edulis Biomass. *Nigerian J Basic Appl Sci* 28: 10–19. https://doi.org/10.4314/njbas.v28i2.2
44. Yadav M, Singh N, Annu, et al. (2024) Recent Advances in Utilizing Lignocellulosic Biomass Materials as Adsorbents for Textile Dye Removal: A Comprehensive Review. *Polymers* 16. https://doi.org/10.3390/polym16172417
45. Mosoarca G, Vancea C, Popa S, et al. (2022) The Use of Bilberry Leaves (Vaccinium myrtillus L.) as an Efficient Adsorbent for Cationic Dye Removal from Aqueous Solutions. *Polymers* 14. https://doi.org/10.3390/polym14050978
46. Kyzas GZ (2012) A Decolorization Technique with Spent "Greek Coffee" Grounds as Zero-Cost Adsorbents for Industrial Textile Wastewaters. *Materials* 5: 2069–2087. https://doi.org/10.3390/ma5112069
47. Karishma S, Deivayanai VC, Thamarai P, et al. (2025) ANN-based modelling and isotherm–kinetic study of dye adsorption on acid-modified manila tamarind seed biomass. *Chem Pap* 79: 7079–7097. https://doi.org/10.1007/s11696-025-04247-6
48. Mihret T, Gabbiye N, Tegegne B, et al. (2025) Removal of reactive red 45 dye from aqueous solution using activated carbon developed from Catha edulis stem as a potential biosorbent. *Sci Rep* 15: 28195. https://doi.org/10.1038/s41598-025-09956-2
49. Wawrzkiewicz M, Bartczak P, Jesionowski T (2017) Enhanced removal of hazardous dye form aqueous solutions and real textile wastewater using bifunctional chitin/lignin biosorbent. *Int J Biol Macromol* 99: 754–764. https://doi.org/10.1016/j.ijbiomac.2017.03.023
50. Khani R, Sobhani S, Beyki MH, et al. (2018) Application of magnetic ionomer for development of very fast and highly efficient uptake of triazo dye Direct Blue 71 form different water samples. *Ecotox Environ Safe* 150: 54–61. https://doi.org/10.1016/j.ecoenv.2017.12.018
51. Biglari H, Gonabad University of Medical Sciences, Gonabad, Iran, Javan N, et al. (2016) Direct Blue 71 Removal from Aqueous Solutions by Adsorption on Pistachio Hull Waste: Equilibrium, Kinetic and Thermodynamic Studies. *Iran J Health Sci* 4: 55–70. https://doi.org/10.18869/acadpub.jhs.4.2.55
52. Strebel A, Behringer M, Hilbig H, et al. (2024) Anionic azo dyes and their removal from textile wastewater through adsorption by various adsorbents: a critical review. *Front Environ Eng* 3. https://doi.org/10.3389/fenve.2024.1347981

53. Giles CH, D'Silva AP, Easton IA (1974) A general treatment and classification of the solute adsorption isotherm part. II. Experimental interpretation. *J Colloid Interface Sci* 47: 766–778. https://doi.org/10.1016/0021-9797(74)90253-7
54. Yu X, Zhang G, Xie C, et al. (2011) Equilibrium, kinetic, and thermodynamic studies of hazardous dye neutral red biosorption by spent corncob substrate. *BioRes* 6: 936–949. https://doi.org/10.15376/biores.6.2.936-949
55. Ouettar L, Guechi E-K, Hamdaoui O, et al. (2023) Biosorption of Triphenyl Methane Dyes (Malachite Green and Crystal Violet) from Aqueous Media by Alfa (Stipa tenacissima L.) Leaf Powder. *Molecules* 28. https://doi.org/10.3390/molecules28083313
56. Foo KY, Hameed BH (2010) Insights into the modeling of adsorption isotherm systems. *Chem Eng J* 156: 2–10. https://doi.org/10.1016/j.cej.2009.09.013
57. Akpa OM, Unuabonah EI (2011) Small-Sample Corrected Akaike Information Criterion: An appropriate statistical tool for ranking of adsorption isotherm models. *Desalination* 272: 20–26. https://doi.org/10.1016/j.desal.2010.12.057
58. Al-Zawahreh K, Al-Degs Y, Barral MT, et al. (2022) Optimization of Direct Blue 71 sorption by organic rich-compost following multilevel multifactor experimental design. *Arab J Chem* 15. https://doi.org/10.1016/j.arabjc.2021.103468
59. Mirzaei N, Mahvi AH, Hossini H (2018) Equilibrium and kinetics studies of Direct blue 71 adsorption from aqueous solutions using modified zeolite. *Adsorpt Sci Technol* 36: 80–94. https://doi.org/10.1177/0263617416684836
60. Reza Moradi (2018) Adsorption of Azo Dye Direct Blue 71 from Aqueous Solution Using NiFe2O4/CP Nanoparticles: Kinetic and Isotherm Model. *Russ J Phys Chem* 92: 2781–2789. https://doi.org/10.1134/S0036024418130277
61. Abbasi M, Habibi MM (2016) Optimization and characterization of Direct Blue 71 removal using nanocomposite of Chitosan-MWCNTs: Central composite design modeling. *J Taiwan Inst Chem Eng* 62: 112–121. https://doi.org/10.1016/j.jtice.2016.01.019
62. Thirunavukkarasu A, Nithya R, Sivashankar R (2021) Continuous fixed-bed biosorption process: A review. *Chem Eng J Adv* 8: 100188. https://doi.org/10.1016/j.ceja.2021.100188
63. Juela D, Vera M, Cruzat C, et al. (2021) Mathematical modeling and numerical simulation of sulfamethoxazole adsorption onto sugarcane bagasse in a fixed-bed column. *Chemosphere* 280: 130687. https://doi.org/10.1016/j.chemosphere.2021.130687
64. Hussein FB, Mayer BK (2022) Fixed-bed column study of phosphate adsorption using immobilized phosphate-binding protein. *Chemosphere* 295: 133908. https://doi.org/10.1016/j.chemosphere.2022.133908



© 2026 the Author(s), licensee AIMS Press. This is an open access article distributed under the terms of the Creative Commons Attribution License (https://creativecommons.org/licenses/by/4.0)